

## SEDIMENT TRANSPORT MODEL FOR THE EOCENE ESCANILLA SEDIMENT-ROUTING SYSTEM: IMPLICATIONS FOR THE UNIQUENESS OF SEQUENCE STRATIGRAPHIC ARCHITECTURES

JOHN J. ARMITAGE,<sup>\*1</sup> PHILIP A. ALLEN,<sup>2</sup> PETER M. BURGESS,<sup>1</sup> GARY J. HAMPSON,<sup>2</sup> ALEXANDER C. WHITTAKER,<sup>2</sup>  
ROBERT A. DULLER,<sup>3</sup> AND NIKOLAS A. MICHAEL<sup>4</sup>

<sup>1</sup>Department of Earth Science, Royal Holloway, University of London, Egham, U.K.

<sup>2</sup>Department of Earth Science and Engineering, Imperial College London, London, U.K.

<sup>3</sup>Department of Earth, Ocean and Ecological Sciences, School of Environmental Sciences, University of Liverpool, Liverpool, U.K.

<sup>4</sup>GTT Division, EXPEC ARC, Saudi Aramco, Dhahran, 31311, Saudi Arabia

**ABSTRACT:** Stratigraphic architectures are fundamentally controlled by the interplay at different temporal and spatial scales of accommodation and sediment supply, modulated by autogenic responses of the sediment routing system and its constituent segments. The flux and caliber of sediment supply is a function of climate, catchment area, and tectonics in the source regions, and unraveling these forcing mechanisms from the observed stratigraphic architecture remains a key research challenge. The mid-to-late Eocene Escanilla sediment routing system had its source regions in the south-central Pyrenean orogen, northern Spain, and transported sediment from wedge-top basins along tectonic strike to marine depocenters. By constructing a volumetric budget of the sedimentary system, it has been demonstrated that there were marked changes in the grain-size distribution released from the sediment sources and also in the position of the gravel front, across three ~ 2.6 Myr time intervals from 41.6 to 33.9 Ma. Classical sequence stratigraphic interpretations would relate the movement of depositional boundaries such as the gravel front to changes of base level, either in isolation or in combination with sediment supply. Herein, we explore the possibility that the position of the gravel front was primarily driven by variability of grain-size distributions released from the source regions as a result of changes in catchment uplift rate and/or surface run-off.

Using a simple model of sediment transport that captures first-order processes, we simulate the lateral movement of gravel deposition in the proximal part of the Escanilla sediment-routing system. Movement of the gravel front is a function of both accommodation generation and the transport capacity of the sediment routing system. We assume that the transport capacity is a linear function of the local slope and the water flux. By assuming that the observed thickness of deposits is equivalent to the accommodation available during deposition, we then use the stratigraphic architecture to constrain the change in catchment size and water flux over the three time intervals of the Escanilla paleo-sediment-routing system. Multiple scenarios are investigated in order to find the most plausible tectonic and climatic history. Model results indicate that during the mid-Eocene there was an increase in catchment length and sediment flux, most likely driven by tectonic uplift in the Pyrenean orogen. Subsequent marked progradation of the gravel front during the late Eocene was the consequence of reduced transport capacity due to a reduction in surface run-off. The latter model result is in agreement with records of pollen taxa that indicate increased climatic aridity in the late Eocene. The combination of a sediment transport model with a full sediment budget makes it possible to test the non-uniqueness of these results.

### INTRODUCTION

The sediment-routing-system concept and sequence stratigraphy provide different, but potentially complementary, approaches to characterize and interpret stratigraphic architectures. Sediment routing systems comprise a sediment cascade from single or multiple source regions to long-term depositional sinks via a series of geomorphic environments characterized by intermittent storage (Burt and Allison 2010). The sequence stratigraphy paradigm is built on the

recognition from subsurface seismic data and surface outcrops of characteristic geometrical relationships, and of their associated expression in vertical successions of strata (e.g., in well logs, cores), in the depositional records of sedimentary basins (e.g., Vail et al. 1977; Galloway 1989; Van Wagoner et al. 1990). There are essentially two unknowns in the sequence stratigraphic model: accommodation and sediment supply (Galloway 1989; Van Wagoner et al. 1990; Heller et al. 1993; Schlager 1993; Carvajal and Steel 2006; Carvajal et al. 2008). Accommodation combines sea level and its equivalent base level in deep-water and nonmarine settings, tectonic subsidence and uplift, syndepositional compaction, and initial topography, and can generally be approximated only from sediment thickness. Sediment supply varies both temporally and spatially, and sets the boundary condition for sediment dispersal in the basin.

\* Present Address: Dynamique des Fluides Géologiques, Université Paris Diderot, Sorbonne Paris Cité, Institut de Physique du Globe de Paris, UMR 7154 CNRS, F-75013 Paris, France

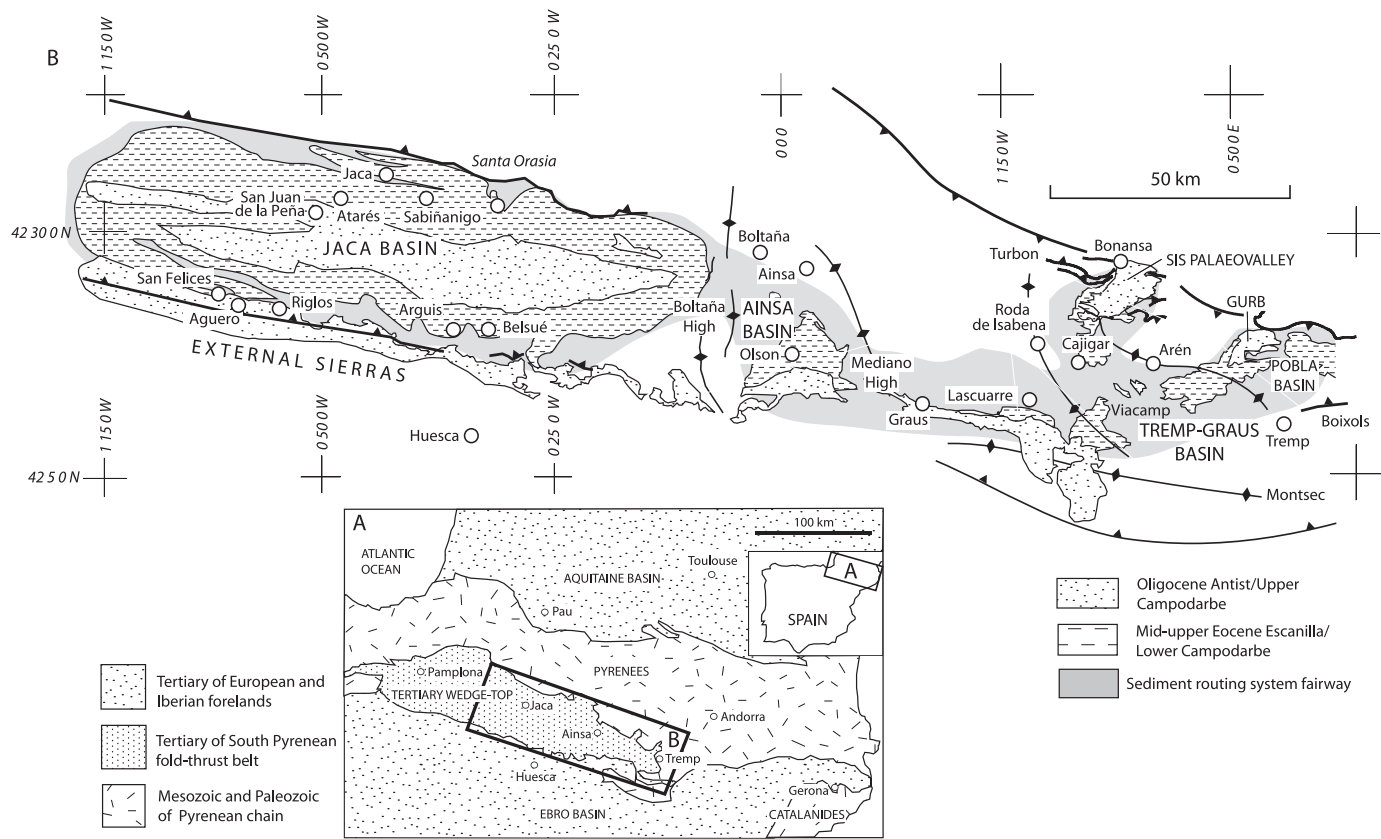


FIG. 1.—A) Location of the Escanilla paleo–sediment-routing system in the Tertiary wedge top of the south-central Pyrenees, northern Spain. B) Detail of the Escanilla paleo–sediment-routing system fairway, after Michael et al. (2014a).

Since accommodation can be estimated from spatial variations in sediment thickness, the ratio of accommodation to sediment supply (A/S ratio) can be qualitatively interpreted from observed stratigraphic architectures (e.g., Muto and Steel 1997; Martinsen et al. 1999). The sediment-routing-system concept is useful in constraining such interpretations of stratigraphic architectures because of its emphasis on sediment flux, which cannot be quantitatively estimated independently of accommodation using classical methods of sequence stratigraphic interpretation. In return, sequence stratigraphic frameworks can provide the stratigraphic context within which coeval segments of sediment routing systems are identified and connected together for further analysis (e.g., Carvajal and Steel 2012).

The grain-size distribution of the sediment supply not only affects rates of downstream fining (Fedele and Paola 2007; Duller et al. 2010), but temporal changes in the grain-size distribution may also generate distinctive stratigraphic architectural patterns (Allen et al. 2015). Consequently, the trajectory of the shoreline or shelf-slope break (Helland-Hansen and Martinsen 1996; Steel and Olsen 2002; Helland-Hansen and Hampson 2009), or of other moving boundaries in the sediment routing system, such as the gravel front (Paola et al. 1992), may be a complex response at different temporal and spatial scales to (i) the volume and grain-size distribution of the sediment supply; and (ii) the rate of generation and spatial distribution of accommodation. A range of numerical modeling and physical experiments has been directed at examining in detail some of the controls on and feedbacks between processes that influence accommodation and sediment supply, and are thus involved in the generation of sequence architectures (Harbaugh et al. 1999; Swenson 2005; Paola et al. 2009; Martin et al. 2009; Armitage et al. 2011). Such studies commonly point to the problem of non-uniqueness in inverting the stratigraphic record for forcing mechanisms (Burgess and Prince 2015). To an extent, the issue of non-uniqueness can be sidestepped by using the A/S ratio as an interpretation tool,

because the various processes that influence accommodation and sediment supply are considered in combination (Muto and Steel 1997; Catuneanu et al. 2009). Although this approach provides a framework for the interpretation of observed stratigraphic architectures (e.g., Martinsen et al. 1999), it does not permit analysis of interactions and feedbacks between processes. Accommodation may also be problematic to define in nonmarine strata, where it is partly dependent on sedimentation (Muto and Steel 2000). Sequence stratigraphic interpretation of such strata, which dominate the proximal portions of stratigraphic sequences and preserved sediment routing systems, relies on concepts that are awkward to test with observational data (e.g., Wright and Marriott 1993; Shanley and McCabe 1994; Holbrook et al. 2006). In practice, temporal variations in the proportion and stacking density of fluvial conglomerate and sandstone bodies are commonly used as a proxy for changes in A/S ratio, with strata characterized by densely stacked conglomerate and sandstone bodies interpreted to have been deposited under low A/S ratios (e.g., Wright and Marriott 1993; Shanley and McCabe 1994). The simplistic, model-driven nature of such interpretations has been highlighted by case studies in which high-resolution dates or paleogeographic variations in sediment thickness allow temporal and spatial variations in accommodation development to be constrained independently of sandstone proportions (e.g., Willis 1993; Giuseppe and Heller 1998). Difficulty in defining accommodation in nonmarine strata further complicates interpretation of sediment supply and the upstream processes that control it in the proximal portions of stratigraphic sequences.

In order to examine the relevance of the sediment-routing-system model for sequence stratigraphic interpretation, we make use of a recently documented case study from the geological record where the sediment budget has been constrained over a period of approximately 8 Myr (Michael 2013; Michael et al. 2013, 2014a, 2014b). The Escanilla sediment-routing system, which spans the Lutetian to Priabonian (41.6–33.9 Ma; Michael et al. 2013), had its source

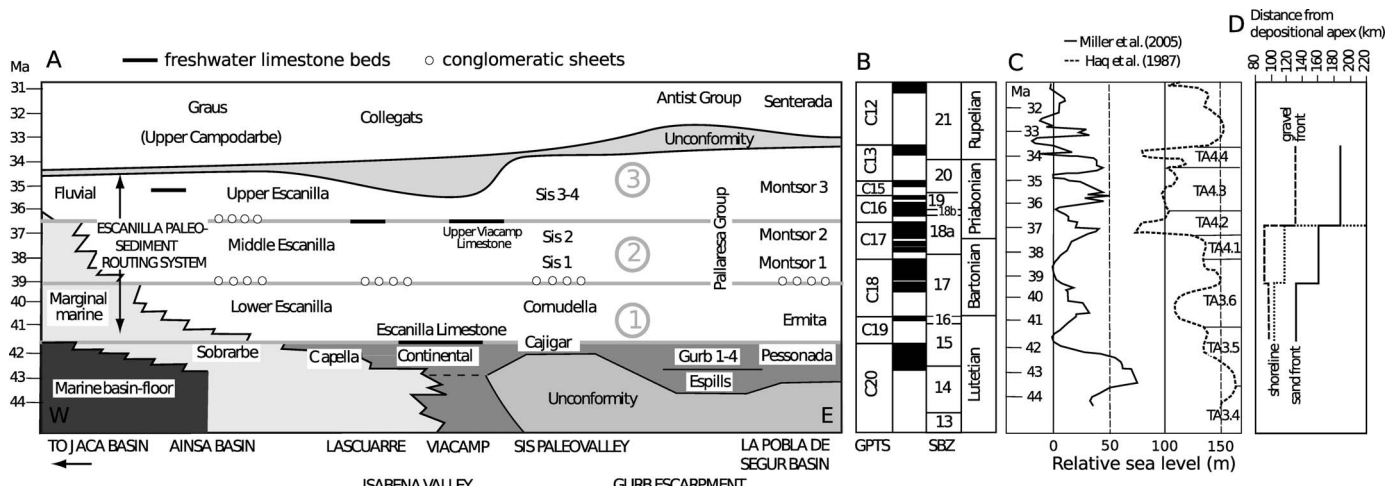


FIG. 2.—A) Summary of the chronostratigraphy of the Escanilla paleo–sediment-routing system in a proximal (right) to distal (left) profile, adapted from Michael et al. (2014a), showing three time intervals. The white circles are conglomeratic sheets, the black horizontal bars are freshwater limestone beds. Both are used to aid correlation. B) Age of the deposits from GPTS, Global Paleomagnetic Time Scale; and SBZ, larger foraminifera shallow benthic zone. C) Global (eustatic) sea-level curves following Haq et al. (1987) and Miller et al. (2005). D) Distance from depositional apex of moving boundaries from Michael et al. (2013) and Michael et al. (2014a).

regions in the south-central Pyrenean orogen, and transported sediment from wedge-top basins along tectonic strike to marine depocenters in the west. The results of the Escanilla study are used to initialize a numerical model for subaerial sediment transport and deposition. We then explore the impact that change in sediment delivery to the basin and change in the capacity of the sedimentary system to transport that sediment has on stratigraphic architecture. The model results test the hypothesis that progradation and retrogradation of moving boundaries, such as the gravel front, can be explained in terms of change in delivery of sediment from source regions. Our work thus examines whether flux of sediment from source regions may be a primary control on observed sequence architectures, particularly in proximal and alluvial regions.

## METHODS

### Sediment Transport

The Escanilla paleo–sediment-routing system can be simplified into two major catchments in the south-central Pyrenees that fed an along-strike series of wedge-top basins (Fig. 1; Michael et al. 2013; Michael et al. 2014a). A third source of sediment, the Santa Orasia system, supplied sediment to the Jaca Basin in the latest Eocene. However, the Santa Orasia source is volumetrically very small, adding less than 25% of the total volume of material supplied to the Jaca Basin and enters the sediment routing system downstream of the main region of gravel fining (Michael et al. 2013; Michael et al. 2014a). The sediment fairway can then be simplified to a single depositional cross section that extends from the Gurb–Pobla and Sis depocenters through the Tremp–Graus, Ainsa, and Jaca basins (Figs. 1, 2; Michael et al. 2013). The relative simplicity of this system allows us to collapse it into a 1-D, upsysterm-to-downsystem profile and to model it as a 1-D system (Figs. 1–3). Our focus is on the proximal part of the sediment routing system, and in particular on movement of the gravel front, since this moving boundary was easy to identify from field-based measurements of particle sizes and grain-size fractions.

### 1-D Sediment Transport Model

To numerically model the 1-D sediment routing system we assume that there is a plentiful supply of transportable sediment. Following Smith and Bretherton (1972) and Simpson and Schlunegger (2003), we then derive a model for

sediment transport that allows the change in surface run-off with depositional length,  $x$  (m), to be accounted for:

$$\partial_t z = U + \partial_x [(\kappa + c q_w^n) \partial_x z] \quad (1)$$

and

$$q_w = \alpha x \quad (2)$$

where  $z$  (m) is elevation,  $U$  ( $\text{m yr}^{-1}$ ) is the spatial distribution of subsidence,  $q_w$  ( $\text{m}^2 \text{yr}^{-1}$ ) is the water flux, and  $\alpha$  ( $\text{m yr}^{-1}$ ) is the precipitation rate. The constants  $\kappa$ ,  $c$ , and  $n$  are explained below. These equations for sediment transport are solved implicitly using a finite-element method with linear weighting functions (see Armitage et al. 2011; Armitage et al. 2014). The model time step is of 10,000 yr, and the model has a spatial resolution of 1-km-long elements. The values of the three constants in the concentrative and dispersive diffusive equation (Equation 1) are controlled by three parameters:  $\kappa$  is a linear diffusion coefficient that is intended to capture all the processes that lead to the rounded curvature of hillslopes,  $c$  is the fluvial incision coefficient and is related to the ability of surface flowing water to transport sediment, and the exponent  $n$ , which has a value greater than 1 (Smith and Bretherton 1972).

The three parameters are difficult to constrain from basic physical principles. The fluvial transport coefficient  $c$  and exponent  $n$  can be upscaled from empirical bed-load transport laws. Assuming Meyer-Peter–Müller bed-load transport laws,  $n \sim 1$ , and following Paola et al. (1992) and Marr et al. (2000) we can estimate that  $0.01 < c \leq 1$ . If, however, we assume  $n = 2$ , which is consistent with the Einstein–Brown formulation of bed-load transport (Simpson and Schlunegger 2003; Densmore et al. 2007; Armitage et al. 2011), then from tuning the model to geological timescales,  $10^{-7} < c \leq 10^{-5} \text{ m}^2 \text{yr}^{-1}$  (see Armitage et al. 2013).

Hillslope processes such as landslides and soil creep can be approximated by a slope-dependent process with diffusion coefficients analogous to  $\kappa$  of order  $10^{-1} \text{ m}^2 \text{yr}^{-1}$  for landslides and  $10^{-4} \text{ m}^2 \text{yr}^{-1}$  for soil creep (Martin and Church 1997). These estimates are derived from short-term observations of less than one hundred years. Classic models of foreland-basin stratigraphic development find that a linear diffusion coefficient of 100 to 5,000  $\text{m}^2 \text{yr}^{-1}$  is more suitable for matching sediment accumulation at geological time scales (Flemings and Jordan 1989; Sinclair et al. 1991). The early diffusive models of Flemings and Jordan (1989) and those that followed lumped both fluvial and hillslope

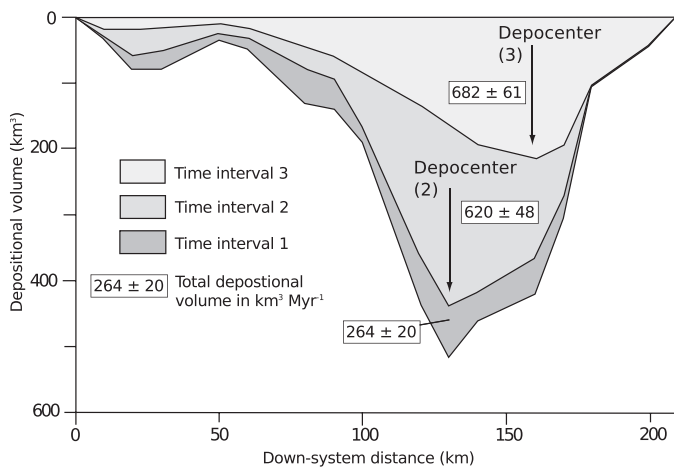


FIG. 3.—Distribution of deposition for the three different time intervals mapped from the Escanilla paleo-sediment-routing system (Michael et al. 2014b).

processes into a single diffusion coefficient, hence the value is much larger than those observed over short timescales. As system length increases, within the framework of Equation 1, the value of  $\kappa$  becomes insignificant compared to the fluvial terms. The effective diffusion coefficient at the outlet of a catchment of length  $L$  is defined by

$$\kappa_{\text{eff}} = \kappa + c(zL)^n \quad (3)$$

The effect of diffusive hillslope processes in the idealized 1-D model becomes important only at the uppermost reaches of the catchment. This is because the hillslope term in Equation 1 becomes important when  $\kappa \sim c/(zx)^n$ , which can be only the case when  $x$  is small, hence applicable only in the headwaters of the catchment.

In order to predict both the area of sediment deposited in the 1-D model and the movement of internal boundaries such as the gravel front, the down-system trends in the grain-size of deposited sediment are calculated. The sediment grain-size distribution is modified down-system by selective deposition following the theoretical model and observations of Fedele and Paola (2007), Duller et al. (2010), and Whittaker et al. (2011). We assume perfect sorting, where only gravel is deposited until it is exhausted, followed by only sand and finally by fine-grained material (silt and clay grade; Paola et al. 1992). This assumption results in a gravel front displaced towards the source region compared to its real-world position where proximal deposits are an admixture of gravel and sand. We examine this effect below by invoking a gravel fractionation coefficient.

Gravel undergoes fining according to an exponential function of Sternberg type (Fedele and Paola 2007; Duller et al. 2010);

$$D(\tilde{x}) = D_{g0} + \varphi_0 \frac{1}{C_v} (e^{-C_g \tilde{y}} - 1). \quad (4)$$

The fining of the sand and smaller grain sizes is given by Sternberg (1875)

$$D(\tilde{x}) = D_{si} e^{-C_s \tilde{y}} \quad (5)$$

In equations 4 and 5  $\tilde{x}$  is the dimensionless down-system length,  $D_{g0} = \log_{10}(D_{50})$  is the median of the gravel input taken from the 50th percentile from Wolman pebble-count data,  $\varphi_0 = \log_{10}(D_{84}/D_{50}) = 0.24$  is the input variance of the gravel assuming that the distribution is log-normal,  $D_{si} = \log_{10}(2 \text{ mm})$  is the initial grain-size for sand and finer material in the sediment input,

TABLE 1.—Data used to initialize the numerical stratigraphic model based on field observations of the Escanilla paleo-sediment-routing system.

Time Interval	Age (Ma)	Duration (Myr)	Gravel Fraction (%)	Sand Fraction (%)	Fines Fraction (%)	Total Volume (km³ Myr⁻¹)
T1	41.6–39.1	2.5	8	23	69	246 ± 20
T2	39.1–36.5	2.6	5	22	73	620 ± 48
T3	36.5–33.9	2.6	13	27	60	713 ± 1
Total	41.6–33.9	7.7	8.8	24.5	66.7	-

and  $\tilde{y}$  is the spatial transformation of the down-system distance given by Paola and Seal (1995);

$$\frac{d\tilde{y}}{d\tilde{x}} = \frac{r(\tilde{x})}{q_s(\tilde{x})}, \quad (6)$$

where  $r(\tilde{x})$  is the down-system distribution of deposition and  $q_s(\tilde{x})$  is the down-system distribution of sediment discharge. In Equations 4 and 5 the coefficients are  $C_v = 0.25$ ,  $C_g = 0.7$  (Fedele and Paola 2007; Duller et al. 2010; Armitage et al. 2011), and  $C_s = 0.3$ . Note that we do not use the self-similar model of Fedele and Paola (2007) for the sand and finer grain sizes, as this would cause there to be no grain sizes larger than the mean for the down-system fining; instead we use the classic “Sternberg model” where the input is the initial grain-size.

#### Derivation of Data for Model Initialization

The Escanilla Formation and time-equivalent strata were divided into three time units based on biostratigraphic and paleomagnetic constraints backed up by sedimentologic logging, paleocurrent analysis, provenance data, and the mapping of distinctive marker horizons such as lacustrine limestones and conglomeratic sheets, as described in Michael et al. (2013), Michael et al. (2014a), and Michael et al. (2014b) (Fig. 2A; Table 1). Absolute ages were obtained using the paleomagnetic standard (Gradstein et al. 2004). The calculation of a sediment budget for the Escanilla sediment-routing system requires the spatial and temporal connection of proximal alluvial fanglomerates with alluvial-plain, coastal, and distal marine deposits. The sediment-routing fairway was mapped and cross-sectional volumes calculated at 23 locations in the down-system direction as described by Michael et al. (2014a). At each location the quantities of gravel conglomerates, sand-grade, and fine-grade fractions were obtained from sedimentological logging. In this way, the down-system pattern of deposited volume, together with the grain-size fraction, was obtained for each of the three time intervals. The position of the gravel cline (where gravel percentages rapidly decline), the gravel front (where gravel is exhausted), and the sand front (where sand is exhausted), are shown in Figure 4 (see Michael et al. 2013).

The location and size of the catchments feeding the Escanilla paleo-sediment-routing system were estimated using a range of provenance indicators (clast lithologies, heavy minerals, U-Pb geochronology of detrital zircons) combined with structural reconstruction of the south-central Pyrenees (Muñoz et al. 2013). The bulk of the sediment of the Escanilla sediment-routing system was derived from two ca. 60-km-long catchments etched into the Axial Zone, which together provided nearly 4000 km³ of particulate sediment over a time period of 7.7 Myr, equivalent to a mean erosion rate of 0.5 to 0.8 mm yr⁻¹ in the source region (Michael et al. 2014b).

The positions of moving boundaries are given in terms of the horizontal distance and in mass-balance coordinates in Table 2 (see Fig. 4; Michael et al. 2013). This mass-balance coordinate system is a spatial transformation of the down-system distance into one that describes the loss of mass (or volume) from that in transport to deposition (Strong et al. 2005; Paola and Martin 2012). To transform the spatial coordinates into a mass-balance coordinate  $\chi$  for any downstream distance, we divide the cumulative depositional

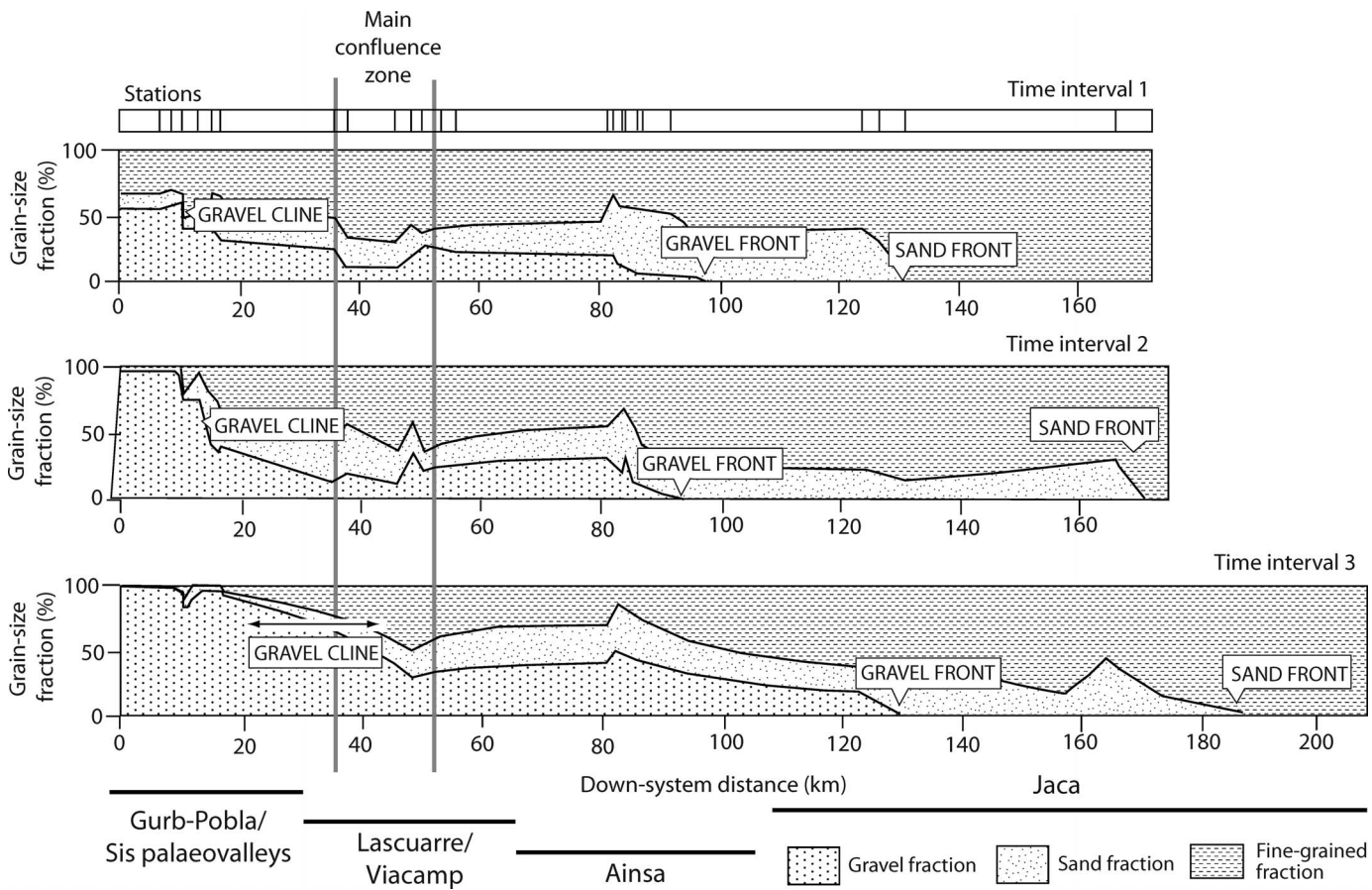


FIG. 4.—Distribution of gravel, sandstones, and fines (siltstones and mudstones) for the three time intervals T1, T2, and T3 (see Table 1; Michael et al. 2013), based on calculation of grain-size fractions at a number of stations distributed in the down-system direction.

volume of sediment at that point by the total depositional volume of the system  $Q_{tot}$ :

$$\chi = \frac{1}{Q_{tot}} \int Q_{dep} dx \quad (7)$$

where  $Q_{dep}$  is the depositional flux at any point  $x$  (see Michael et al. 2013). Inspection of Figure 4 and Table 2 shows that the gravel front does indeed retreat slightly during time interval 2 at the same time as the percentage gravel fraction in the supply also decreases (Table 3).

The numerical model fines the sediment assuming a single mean grain-size in the sediment supply. It first fines gravel clasts and once there is no gravel left the model fines the remaining volume of material assuming that it is made of sand and finer grain-sizes only. This perfect sorting (cf. Paola et al. 1992), however, is idealized. To compare the model to observations, a gravel fractionation coefficient can be defined that represents the total cumulative volume of sediment deposited at the gravel front compared to the volume of gravel in the supply (alternatively, the distance to the observed gravel front compared to the theoretical distance assuming perfect sorting). We can then use this coefficient as a first-order method to adjust the observed gravel front to where it would be assuming perfect sorting (see Section 3.1). The fractionation coefficient varies between 2.3 and 3.8 (Table 3), indicating rather poor efficiency of fractionation of different grain sizes.

#### External Forcing, Boundary, and Initial Conditions

The numerical model is subject to external forcing in the form of a distribution of subsidence that varies in space and time, a flux of sediment from the

catchment on the left boundary and a precipitation rate within the model domain and catchment. The model domain is 1000 km long. The initial condition is a linear topographic profile with an elevation of 500 m on the left boundary and 0 m on the right boundary. The right boundary is of fixed elevation at 0 km. The left boundary has an influx of sediment (either 12 or 20  $m^2 \text{ yr}^{-1}$ , see Table 4). Before applying the model to the history of the Escanilla paleo-sediment-routing system we allow for a 5 Myr model wind-up time, as this is sufficient time to allow the model topography to evolve towards the equilibrium profile (Armitage et al. 2011).

After the 5 Myr model wind-up time, we impose a subsidence rate that changes through the three time intervals with model time spans of T1, 5–7.5 Myr; T2, 7.5–10.1 Myr; T3, 10.1–12.7 Myr. The profile of subsidence is estimated by interpolating, using a spline function, between the measured thickness of the deposits at specific locations down-system (Michael et al. 2014b; Fig. 3). To understand how change in the various model parameters impacts the movement of the gravel front and the depositional architecture, we first systematically vary  $\kappa$ ,  $c$ , and  $n$  in Equation 1 (Table 4). In the following section we vary the precipitation rate, catchment length, and distribution of grain-size in the gravel input (Table 4). We make the simple assumption that the input sediment flux for each time interval is equal to the total volume per million years deposited within the basin (Table 1). For the simple 1-D model, the volume flux needs to be converted into an area flux. To do so we assume that the width of the outlet at the left boundary of the model is 20 km, representing the combination of two catchments providing sediment to the basin. This allows a sediment influx of 12, 31, and 34  $m^2 \text{ yr}^{-1}$  during time intervals T1, T2, and T3 to be approximated (Table 4). The numerical model also incorporates a headward expansion of the catchments over time from 40 km in T1 to 60 km in T2 and

TABLE 2.—Position of moving boundaries from a field study of the Escanilla paleo-sediment-routing system in terms of horizontal distance from the apex of the depositional system and in mass-balance coordinates. Data are from Michael (2013) and Michael et al. (2013).

Time Interval	Gravel Cline (km)	Gravel Front (km)	Sand Front (km)	Depositional Length (km)
T1	10	95	130	165
T2	17	90	165	175
T3	30	130	185	210
Total mass balance co-ordinate $\chi$				
T1	0.010	0.38	0.7	1
T2	0.015	0.14	1	1
T3	0.030	0.38	1	1

T3 (Table 4) as suggested from provenance data summarized in Michael et al. (2014b) and consistent with previously inferred tectonic movements in the Pyrenean Orogen (Marzo and Steel 2000).

Finally, we then run through the parameter space to find the combination of parameters that best fits the observed location of the gravel front. The model assumes perfect sorting, that is, the grain-size deposited at a model point refers to mean gravel, mean sand, and mean fines. Consequently, when assessing the representativeness of model simulations, the predicted location of the gravel front is different from that which is observed. The comparison of model prediction and field observation of the position of the gravel front is facilitated by transforming the spatial coordinates into mass-balance coordinates and then adjusting the observed location of the gravel front assuming that only gravel is deposited first. The model parameters can then be selected that match this adjusted position. The implications of the best-fit model are then discussed with reference to stratigraphic observations and interpretations.

## RESULTS

### Effect of Model Parameters on Depositional Architecture

The effect of changing the three model parameters ( $\kappa$ , the linear diffusion coefficient,  $c$ , the transport coefficient and  $n$ , the exponent on the water flux) on the deposition of sediment in terms of grain-size is displayed in Figure 5. It is immediately apparent that change in the linear diffusion coefficient over four orders of magnitude has no impact on the depositional volumes and the

TABLE 3.—Volumes of grain-size fractions in the Escanilla paleo-sediment-routing system. The gravel fractionation coefficient is the measured position of the gravel front compared to the theoretical position for perfect sorting, measured in the mass-balance coordinate. Data are from Michael (2013) and Michael et al. (2013).

Time Interval	Volume Gravel ( $\text{km}^3 \text{Myr}^{-1}$ )	Volume Sands ( $\text{km}^3 \text{Myr}^{-1}$ )	Volume Fines ( $\text{km}^3 \text{Myr}^{-1}$ )	Gravel Fractionation Coefficient
T1	19	57	170	2.5
T2	29	134	456	2.3
T3	87	188	407	3.8

distribution of gravel and finer-grained deposits (Fig. 5A–C). This is because at large distances, throughout the depositional area, the water flux-dependent part of the model equations dominate. The linear diffusion term becomes dominant only in the very proximal part of the erosional profile. Therefore, in all runs beyond this first trio (Fig. 5A–C) we simply set  $\kappa = 1 \text{ m}^2 \text{ yr}^{-1}$ .

In contrast, change in the transport coefficient  $c$  has a large impact on the distribution of gravel and finer grain deposits within the depositional realm (Fig. 5D–I). An increase in the transport capacity causes the gravel front and sand front (contoured as 1.75 mm grain-size) in all three time intervals to migrate farther down-system. Changing the value of  $n$  likewise shifts the location of the gravel front, yet there is a trade-off with the value of  $c$  such that the appropriate combination of values of  $n$  and  $c$  can achieve similar results in the down-system grain-size distribution. However, changes in  $c$  have a stronger effect than variations in  $n$ .

The gravel front of the Escanilla paleo-sediment-routing system is located at between 90 and 130 km distance down-system from the depositional apex during the three time intervals (Figs. 2, 4, Table 2). Using the mass-balance framework we then calculated the fractionation coefficient by comparing the position of the gravel front for perfect sorting to the observed position (Table 3). By calculating the cumulative integral of deposition in the model, the transformation of the perfect-sorting gravel front in mass-balance space ( $\chi$ ; Table 3) to spatial coordinates can then be calculated (Table 5). Using this as a guide, a transport model with  $n = 1$  and  $c = 0.1$  gives a reasonable location of the gravel front at between 25 and 100 km. A transport model with  $n = 2$  and  $c = 10^{-5} \text{ m}^{-2} \text{ yr}^{-1}$  likewise gives a reasonable location of the gravel front at between 40 and 100 km.

TABLE 4.—Model names and parameters;  $n$ , exponent on water flux;  $c$ , fluvial transport coefficient;  $\kappa$ , linear diffusion coefficient;  $q_{s(in)}$ , influx of sediment at the left boundary;  $\alpha$ , precipitation rate;  $l_c$ , catchment length;  $D_{go}$ , mean grain-size of gravel input.

Parameter Units	$n$	$C$ ( $\text{m}^2 \text{yr}^{-1}$ ) $^{1-n}$	$K$ $\text{m}^2 \text{yr}^{-1}$	Time Interval T1				Time Interval T2				Time Interval T3			
				$q_{s(in)}$ $\text{m}^2 \text{yr}^{-1}$	$\alpha$ $\text{m yr}^{-1}$	$l_c$ km	$D_0$ mm	$q_{s(in)}$ $\text{m}^2 \text{yr}^{-1}$	$\alpha$ $\text{m yr}^{-1}$	$l_c$ km	$D_0$ mm	$q_{s(in)}$ $\text{m}^2 \text{yr}^{-1}$	$\alpha$ $\text{m yr}^{-1}$	$l_c$ km	$D_0$ mm
Figure 4															
	1	0.1	0.01	20	0.2	40	40	20	0.2	40	40	20	0.2	40	40
	1	0.1	1	20	0.2	40	40	20	0.2	40	40	20	0.2	40	40
	1	0.1	1	20	0.2	40	40	20	0.2	40	40	20	0.2	40	40
	1	0.01	1	20	0.2	40	40	20	0.2	40	40	20	0.2	40	40
	1	1.0	1	20	0.2	40	40	20	0.2	40	40	20	0.2	40	40
	2	$10^{-5}$	1	20	0.2	40	40	20	0.2	40	40	20	0.2	40	40
	2	$10^{-6}$	1	20	0.2	40	40	20	0.2	40	40	20	0.2	40	40
	2	$10^{-7}$	1	20	0.2	40	40	20	0.2	40	40	20	0.2	40	40
Figure 5															
M1A	1	0.1	1	12	0.2	40	40	31	0.2	40	40	34	0.2	40	40
M1B	1	0.1	1	12	0.2	40	24	31	0.2	40	46	34'	0.2	40	42
M1C	1	0.1	1	12	0.2	40	24	31	0.4	60	46	34	0.4	60	42
M2A	2	$10^{-5}$	1	12	0.2	40	40	31	0.2	40	40	34	0.2	40	40
M2B	2	$10^{-5}$	1	12	0.2	40	24	31	0.2	40	46	34	0.2	40	42
M2C	2	$10^{-5}$	1	12	0.2	40	24	31	0.4	60	46	34	0.4	60	42

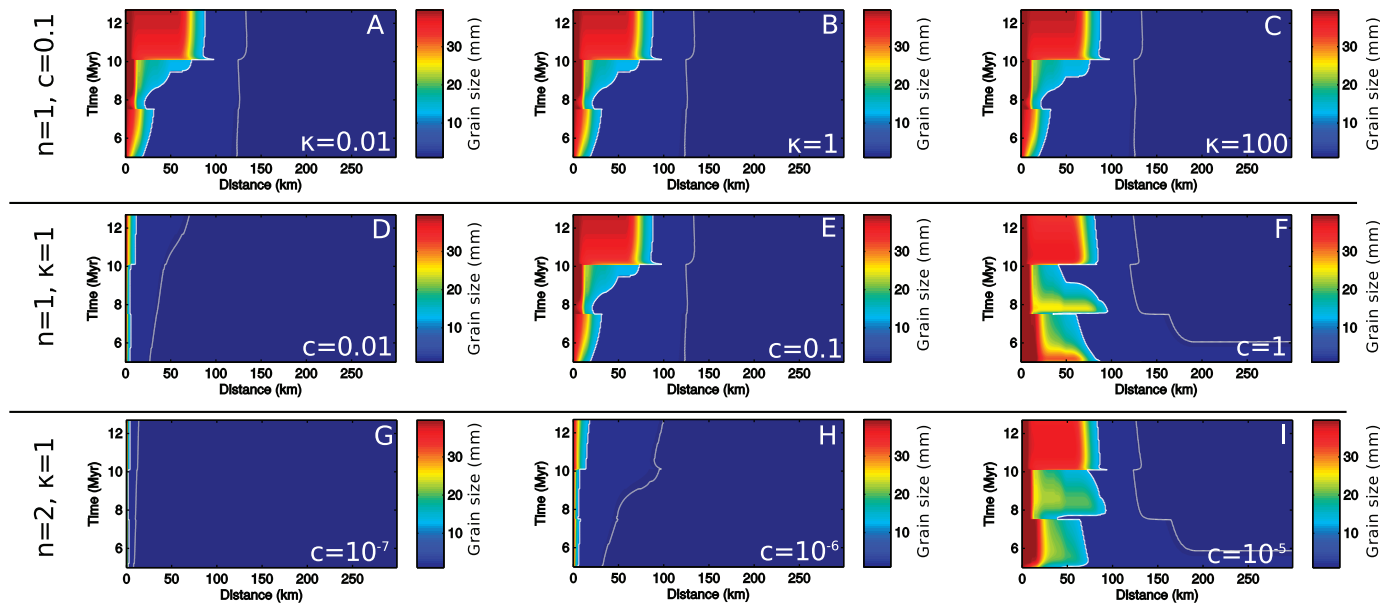


FIG. 5.—Wheeler diagrams of the grain-size (in mm) deposited in the idealized Escanilla sediment-routing system to compare model output for the parameters in Table 4. In parts A to C the linear diffusion coefficient  $\kappa$  is varied from  $0.01$  to  $100 \text{ m}^2 \text{ yr}^{-1}$ , while  $n = 1$  and  $c = 0.1$ . In Parts D to F the transport coefficient  $c$  is varied from  $0.01$  to  $1$ , while  $n = 1$  and  $\kappa = 1 \text{ m}^2 \text{ yr}^{-1}$ . In Parts G to I the transport coefficient  $c$  is varied from  $10^{-7}$  to  $10^{-5} \text{ m}^{-2} \text{ yr}$  while  $n = 2$  and  $\kappa = 1 \text{ m}^2 \text{ yr}^{-1}$ . The location of the idealized gravel front due to perfect sorting is given by the white contour. The gray contour plots 1.75 mm grain-size.

#### *Effect of Change in the Characteristics of the Sediment Supply*

The predicted depositional architecture is a function of both the model parameters (Fig. 5) and the boundary conditions (Fig. 6). From the volumetric budget of sediment deposited in the Escanilla system we first explore how the model responds to a change in flux of the sediment supply as it undertakes the transitions from time interval T1 to T2, and from T2 to T3 (Fig. 6A, D, G, J; models M1A and M2A in Table 4). The result of increasing the sediment flux from  $12$  to  $31 \text{ m}^2 \text{ yr}^{-1}$  from T1 to T2 is to transiently reduce the distance to which gravel and finer grain sizes are deposited, as the increased flux requires increasing slope at the left boundary, thereby increasing the thickness of deposits at short distances down-system. The position of the gravel front and sand front (1.75 mm grain-size contour) at the beginning of time interval T2 is reduced to only a few kilometers from the apex (Fig. 6A, G). For the two models M1A and M2A, in mass-balance coordinates the locations of the gravel and sand fronts do not move significantly from time interval T1 to T2, because the ratio of input flux to accommodation space is similar (Fig. 6D, J). From time interval T2 to T3 there is then progradation of the gravel front as supply increases relative to accommodation and the system recovers towards the topographic steady-state that balances the input sediment flux and the distribution of subsidence (Fig. 6A, G).

The addition of a change in the gravel grain-size distribution of the sediment supply (models M1B and M2B) does not change the location of the gravel front because the total fraction of gravel entering the basin has not changed (Fig. 6B, E, H, K). It does, however, alter the interpretation of the gravel cline, because during time interval T1 there is a smaller quantity of coarse material

entering the basin relative to T2 and T3. The subsequent addition of an increase in precipitation rate from  $0.2$  to  $0.4 \text{ m yr}^{-1}$  and an expansion of the catchment length from  $40$  to  $60 \text{ km}$  from time interval T1 to T2 have a dramatic effect on the position of the gravel front and the sand front (Fig. 6C, F, I, L; models M1C ad M2C). Farther models show that this shift in deposition is primarily due to change in precipitation rate, because this affects the water flux in both the catchment acting as a source region and in the depositional segment, whereas an increase in catchment length only increases the water flux leaving the source region.

Increasing the precipitation rate from  $0.2$  to  $0.4 \text{ m yr}^{-1}$  increases the sediment transport capacity as the model undergoes the transition from time interval T1 to T2. This increased transport capacity lowers slope at the input (left) boundary and therefore reduces the change in elevation at this boundary due to the increased input of sediment from T1 to T2. The response is a progradation of coarse material during time interval T2 as the larger input of material is deposited as a thinner wedge down-system (Fig. 6C, I). The effect is strongest when  $n = 2$ , as in this case the transport is a function of precipitation rate multiplied by down-system length squared. For model M1C where  $n = 1$ , the gravel front is located between  $25$  and  $90 \text{ km}$ , with a progradation during time interval T3 to  $90 \text{ km}$  (Fig. 6C). For model M2C where  $n = 2$ , the gravel front varies between  $50$  and  $100 \text{ km}$  with a marked progradation during the early part of time interval T2 (Fig. 6I).

The combined effects of changes in the flux of the sediment supply and the transport capacity cause marked shifts in the deposition of gravel and sand. While providing information on the temporal evolution of the gravel front and gravel cline, the Wheeler diagrams in Figures 5 and 6 do not show the thickness of deposits. Models M1C and M2C are likely the most realistic because they take into account the widest set of observational constraints. The stratigraphic architecture predicted by these two models shows a thickening of deposits down-system of  $100 \text{ km}$  (Fig. 7), which is consistent with field observations and is driven by the down-system increase of subsidence that creates more accommodation in this region. If we assume  $n = 1$  in the transport equations (model M1C), then there is some erosion of the proximal  $50 \text{ km}$  of deposits within time interval T1 (Fig. 7C). An area corresponding to  $4 \times 10^4 \text{ m}^2$  is eroded off the most proximal deposits of time interval T1. Other than this erosion, the stratigraphic architecture is similar to that observed. If,

TABLE 5.—Observed gravel front and the location of the gravel front adjusted for perfect sorting.

Time Interval	Observed Gravel Front (km)	Fraction Coefficient	Perfect Sorting Gravel Front (km)
T1	95	2.5	58
T2	90	2.3	40
T3	130	3.8	78

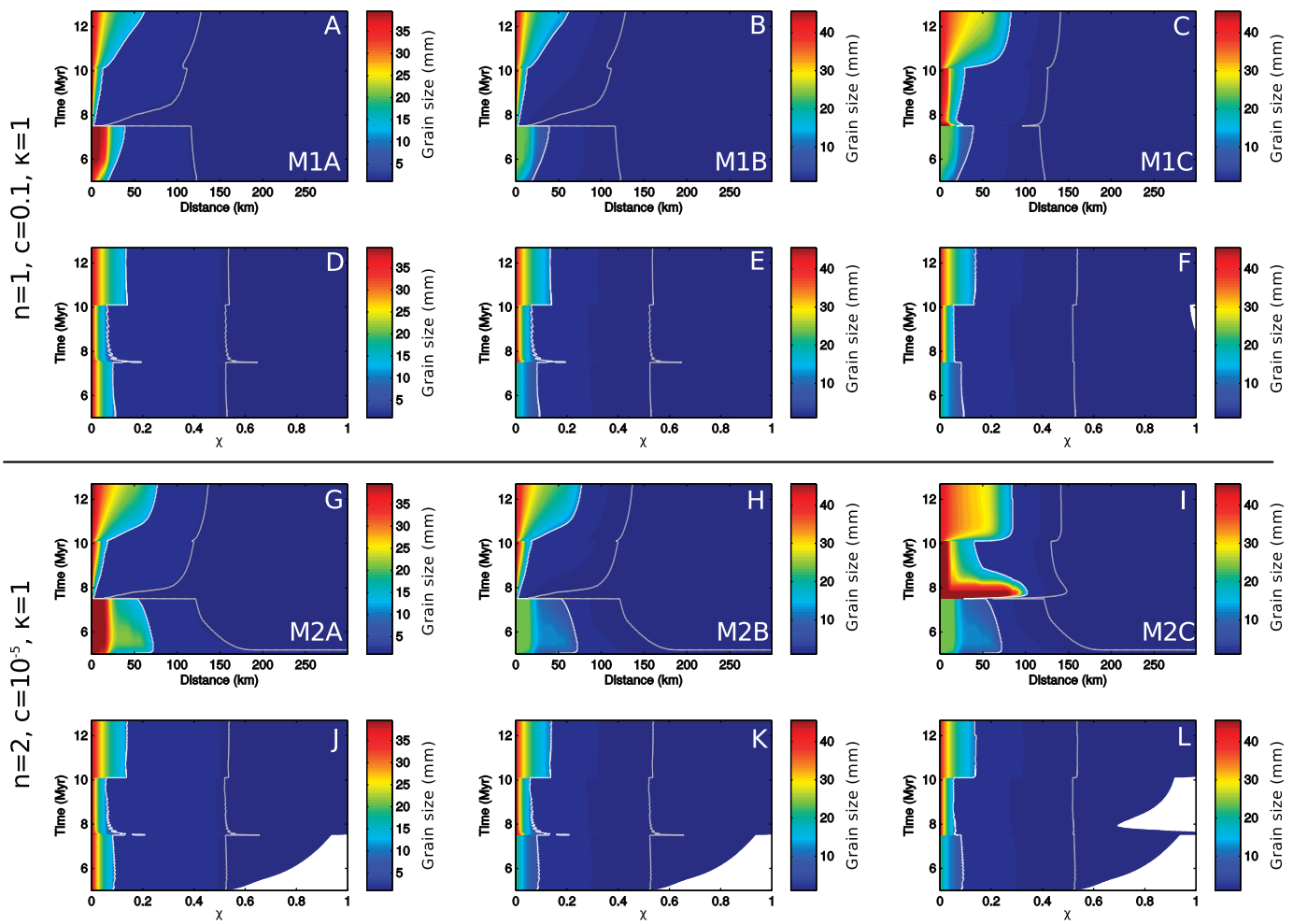


FIG. 6.—Wheeler diagrams of the grain-size (in mm) deposited in the idealized Escanilla paleo–sediment-routing system and the same information transformed into mass-balance coordinates  $\chi$ . The models displayed correspond to the parameter combinations given in the lower part of Table 4. Parts A to F show the results for models in which  $n = 1$ ,  $c = 0.1$  and  $\kappa = 1 \text{ m}^2 \text{ yr}^{-1}$ . Parts G to L show the results for models in which  $n = 2$ ,  $c = 10^{-5} \text{ m}^{-2} \text{ yr}^{-1}$  and  $\kappa = 1 \text{ m}^2 \text{ yr}^{-1}$ . From left to right: Models M1A and M2A, which include a change in input sediment flux during time intervals T1, T2, and T3. Models M1B and M2B also include a change in the mean grain-size entering the basin. Models M1C and M2C also include a change in catchment length and precipitation rate. The location of the idealized gravel front due to perfect sorting is given by the white contour. The gray contour plots the 1.75 mm grain-size. The white space in Parts J to L display the regions where  $\chi$  does not reach 1 in the down-system direction because of basin bypass, i.e., the basin is not closed and so mass is lost.

however,  $n = 2$  (model M2C) then there is significant erosion of the uppermost deposits from time interval T1, so that  $5 \times 10^6 \text{ m}^2$  of deposits are eroded between down-system distances of 0 and 50 km (Fig. 7D). Such erosion is not documented in the Escanilla sediment routing system, which suggests that the transport efficiency of the model with  $n = 2$  is too high to offer a realistic set of solutions. Furthermore, in models with  $n = 2$  there is an unreasonable amount of basin sediment bypass beyond the basin margin represented by the lower model boundary, as shown by the periods where the flux out of the basin is greater than zero, and recorded by the mass-balance coordinate  $\chi$  not reaching 1 (Figs. 5J–L, 6B).

#### Finding a Best-Fit Model

To find the parameters and boundary conditions that best match the observed stratigraphic record of the Escanilla paleo–sediment-routing system, it is necessary to find a model run that simulates the correct location of the gravel front in each time period (Table 5). It is also necessary to find a model run that has minimal sediment bypass beyond the basin limit, as the implicit assumption is that the sediment budget of the Escanilla paleo–sediment-routing system is closed (Michael et al. 2013, 2014b). It has already been shown that a change

in the linear diffusivity,  $\kappa$ , has very little effect on the stratigraphic architecture (Fig. 5A–C). This parameter is therefore fixed at  $1 \text{ m}^2 \text{ yr}^{-1}$ . Furthermore, the case where  $n = 1$  is preferred, because when  $n = 2$  the high transport efficiency leads to both proximal erosion and a significant amount of sediment bypass beyond the basin limit (Figs. 5J–L, 6B, D).

The procedure used to find the best-fit model is illustrated in Figure 8. Two parameters are varied that have the largest influence on the position of the gravel front: precipitation rate,  $\alpha$ , and the transport coefficient,  $c$ . Starting with time interval T1, one hundred simulations were run, varying both precipitation rate and the transport coefficient (Fig. 8A, B). We then compare the predicted maximum location of the gravel front and the location of the observed gravel front adjusted for perfect sorting (Table 5). In Figure 8 the ratio of the amount of sediment that leaves the model domain compared to the input sediment flux is plotted, to check that the model with the matching gravel front does not produce significant bypass of sediment.

We find that the best fit for time interval T1 occurs when the precipitation rate  $\alpha = 0.19 \text{ m yr}^{-1}$  and the transport coefficient  $c = 0.17$ . The best-fit values of precipitation rate and transport coefficient are then used to model both the wind-up period of 5 Myr and time interval T1. These two parameters were then changed for time interval T2 (Fig. 8B, C). The best-fit model for the

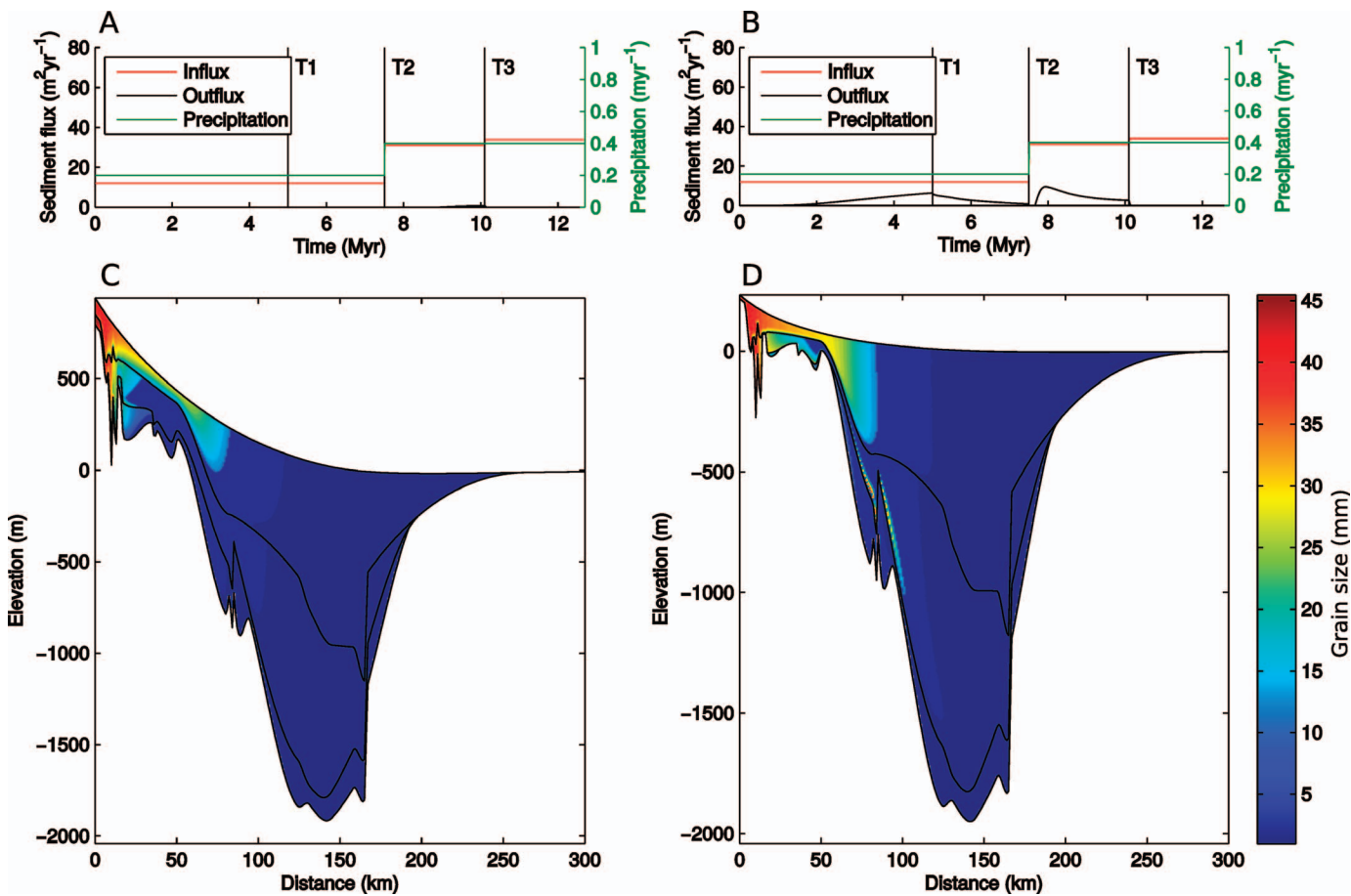


FIG. 7.—Stratigraphy for models M1C and M2C in Table 4. **A)** Input sediment flux, sediment flux out at the lower model boundary (at 1000 km), and precipitation rate plotted against time for model M1C. The 5 Myr wind up time is shown followed by three time intervals, T1, T2, and T3. **B)** As in Part A but for model M2C. **C)** Grain-size of sediment deposited plotted at the end of the model M1C run showing the modeled stratigraphy for the three time intervals. The stratigraphy for the wind-up period is not shown. **D)** As in Part C but for model M2C.

location of the adjusted gravel front is found to be when the transport coefficient  $c = 0.17$ . However, precipitation rates are required to increase to  $\alpha = 0.41 \text{ m yr}^{-1}$  (Fig. 8A, B). There is a small amount of sediment bypass beyond the basin under these conditions. Next, the model is restarted using the best-fit parameters for both time intervals T1 and T2 and the range of precipitation and transport coefficient for time interval T3 is tested. Once again, the transport coefficient that best matches the location of the gravel front is  $c = 0.17$ , accompanied by a reduction in precipitation rate to  $\alpha = 0.23 \text{ m yr}^{-1}$  (Fig. 8A, B).

The location of the gravel front is controlled by the distribution of accommodation and the transport of material down-slope. When the location of the gravel front is plotted against the product of precipitation rate and transport coefficient (Fig. 8C) the trend has a complex functional form that is dependent on the distribution of accommodation. However, a clear trend is observed, suggesting that there is a unique transport capacity that gives rise to the location of the gravel front when combined with the distribution of accommodation. The transport coefficient  $c$  can be estimated from first principles under the assumption  $n = 1$  (Paola et al. 1992). Depending on the grain size in transport,  $0.1 < c < 1$  (Marr et al. 2000; Paola et al. 1992). In a previous numerical model it was found that for the transport of sediment over very long distances  $c \sim 0.01$  (Armitage et al. 2014). For the Escanilla sediment routing system we find that  $c = 0.17$ , which is within the range of estimates of  $c$  derived from first principles (Marr et al. 2000; Paola et al. 1992).

## DISCUSSION

### *The Escanilla Paleo-Sediment-Routing System and Predicted Stratigraphy*

The duration of the Escanilla paleo-sediment-routing system spans the Lutetian to Priabonian stages of the Eocene (41.6–33.9 Ma; Michael et al. 2013, 2014a). Over this time period, there was an overall progradation of facies belts to the west, along the strike of the central Pyrenean orogen. Fluvial environments persisted in the eastern sector of the sediment-routing system in the mid-to-late Eocene (Muñoz 1992; Puigdefàbregas et al. 1992; Bentham and Burbank 1996), sourced from the internal zones of the south-central Pyrenees. Fluvial systems in the east supplied deltaic coasts, shallow marine environments, and pro-delta slopes in the Ainsa Basin and deep marine basin floor environments in the Jaca Basin to the east (Nijman 1998; Dreyer et al. 1999) (Fig. 2). The sediments of the alluvial segment are therefore linked with coeval marine deposits to the east, the shoreline migrating a distance of approximately 100 km between time interval T1 and time interval T3. The gravel and sand fronts also migrate westwards over time, but the gravel front retreats slightly during time interval T2, independent of the overall progradation of the system. In the Escanilla paleo-sediment-routing system the eustatic sea-level curves do not correspond to observed stratigraphic boundaries and architectures in the Escanilla routing system (Fig. 2), due, at least in part, to locally variable tectonic subsidence in the Pyrenean foreland basins (e.g., Marzo and Steel 2000).

Regional and proxy data, which are independent of outcrop observations, can be used to constrain climate, hinterland tectonics, and relative sea level

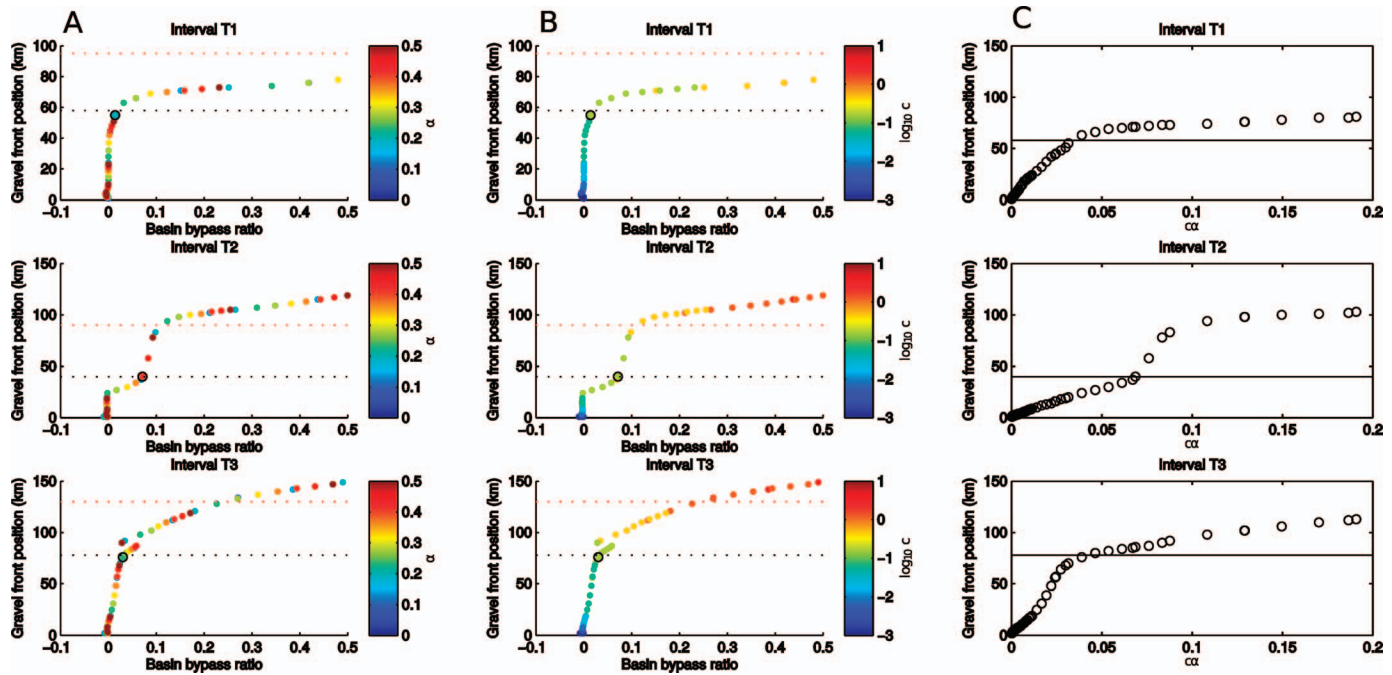


FIG. 8.—Scatter plots of the basin bypass ratio, defined as the ratio of sediment flux out of the basin to sediment influx, against the maximum distance that the gravel front reaches for different precipitation rates and transport coefficients during the time intervals T1, T2, and T3. A) Scatter plot of gravel front vs. bypass for the three model time intervals. The colors are for different values of precipitation rate. The red dotted line is the location of the gravel front, and the black dotted line is the location of the gravel front adjusted for perfect sorting. The black circle shows the best-fit model for the particular time interval. B) As in Part A, but the color scale shows the transport coefficient. C) Scatter plot of the product of the transport coefficient  $c$  and precipitation rate  $\alpha$ . The black line is the location of the adjusted gravel front. It can be seen that there is an ideal combination of precipitation and transport coefficient that gives a match to the adjusted location of the gravel front.

during the mid-Eocene to the basal Oligocene, in order to test the viability of the best-fit model (Fig. 9). During time intervals T1 and T2 the location of the gravel front contracts slightly from 58 to 40 km when adjusted for perfect sorting (Table 5). Subsidence rates inferred from depositional thicknesses, however, increase by up to a factor of four from time interval T1 to interval T2 (Fig. 3). The sediment flux entering the basin is likewise increased by a factor of three to match the volume of sediment deposited. In the absence of a change in precipitation, the position of the gravel front would decrease to < 25 km (Fig. 6A, B, G, H). An increase in the precipitation rate and hence transport capacity reduces the slope and hence the elevation at the catchment outlet at the left boundary of the model, and sets the gravel front at 40 km down-system. The increase in precipitation is therefore required to prevent significant retreat of the gravel front.

The migration of the shoreline during the Bartonian to Priabonian is shown in Figure 2D. The transition from deltaic to fluvial deposits in the Jaca and Ainsa basins records progradation of the Escanilla paleo-sediment-routing system during this time interval, and has been attributed to a fall in base level by some authors (Bentham et al. 1992). Evidence from thermochronology suggests that erosion of the hinterland regions was relatively steady at between 0.25 to 0.3 mm yr<sup>-1</sup> in the mid-to-late Eocene, increasing to > 1 mm yr<sup>-1</sup> in the latest Eocene–early Oligocene (after time interval T3), as uplift continued in the Axial Zone (e.g., Beamud et al. 2010; Whitchurch et al. 2011; Michael et al. 2014b). Palynological data from the Ebro Basin indicate that in the middle Bartonian the climate was very warm and humid, suggesting high precipitation rates at the transition from T1 to T2 (Cavagnetto and Anadón 1996). Therefore, it is possible that increased sediment flux due to increased runoff led to the change in the position of the gravel front without requiring base-level change.

The gravel front migrated from 40 to 78 km down-system in time interval T3 when adjusted for perfect sorting (Table 5). Progradation of the gravel front occurred in part due to the change in the distribution of accommodation, as

displayed by the models where input sediment flux and precipitation do not vary significantly between T2 and T3 (Fig. 6). In these models the gravel front is located at approximately 100 km or more down-system (Figs. 5, 6). To account for the adjusted observed location of the gravel front while maintaining the flux required to match the observed deposited volume, a reduction in transport capacity is required. This is best achieved through a reduction in precipitation rates from roughly 0.4 to 0.2 m yr<sup>-1</sup> (Fig. 9). The record from pollen taxa indicates that there was a transition to more open vegetation in the Priabonian (Cavagnetto and Anadón 1996). The implications of our sediment transport model are therefore consistent with palynological evidence that the climate became drier during time interval T3.

The model simulates propagation of the gravel front during time intervals T1 and T2 followed by a cycle of retrogradation and subsequent progradation during time interval T3 (Fig. 9). Synthetic sedimentary logs can be extracted from different distances along the model length to show how these responses to changing sediment supply and precipitation rate may be recorded in stratigraphy (Fig. 10). The synthetic logs show that close to the catchment outlets (10–20 km from the depositional apex) the stratigraphy is simulated to be dominated by gravel, as observed within the Pobla Basin and Sis Paleovalley (Figs. 1, 9A; Michael et al. 2014b). Farther down-system in the Tremp (Lascuarre locality at 40–60 km) and Ainsa (70–90 km) basins (Fig. 1), the synthetic logs allow the model predictions to be compared to observations recorded in measured logs (Michael et al. 2014b). To make this comparison, the observed sedimentary logs are filtered using a Gaussian filter with a window of 50 m in order to highlight the large-scale trend. The filtered logs from the Lascuarre area and Ainsa Basin show deposition of mainly sandstones and fine-grade sediments during intervals T1 and T2 (Fig. 10). It is only towards the end of time interval T3 that there was significant gravel deposition with clast sizes of 20 mm in the Lascuarre log (Vincent 2001; Fig. 10B). The Ainsa log likewise shows that there was significant gravel conglomerate deposition only during the later part of time interval T3 (Fig. 10C).

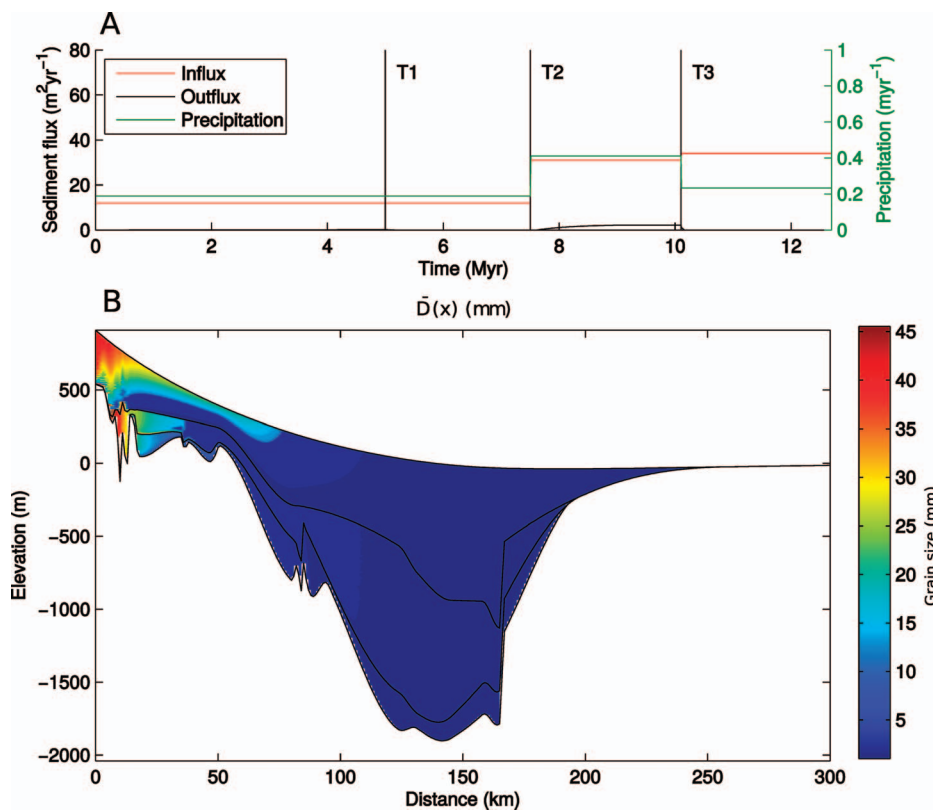


FIG. 9.—Stratigraphic architecture predicted by the forward model run that most closely matches the observed location of the gravel front adjusted for perfect sorting. **A)** Sediment flux in and out of the basin and precipitation rate against time. **B)** Distribution of grain-size deposited in the idealized Escanilla paleo-sediment-routing system.

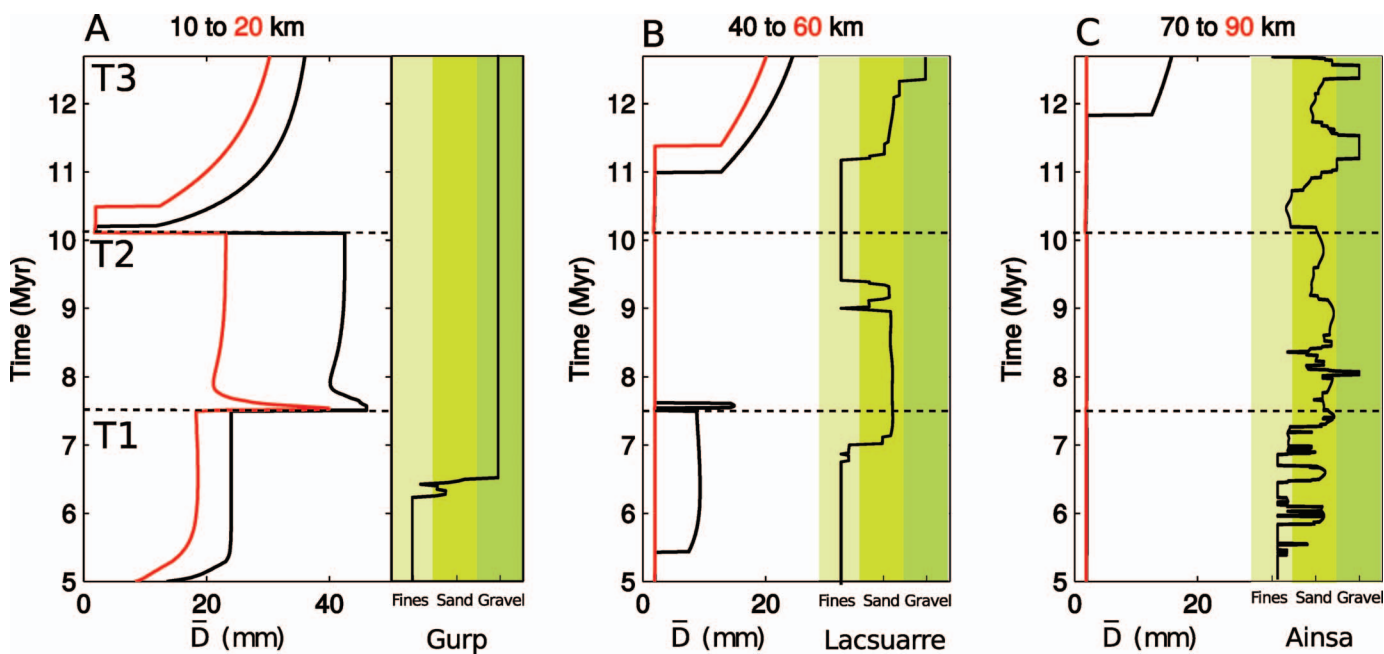


FIG. 10.—Synthetic sedimentary logs taken at six distances down the system (see Fig. 9). **A)** Logs at 10 (black) and 20 km (red) distance down-system. Also displayed is a filtered sedimentary log taken from the Gurb escarpment in the Pobla Basin (Fig. 1; Michael et al. 2014b). **B)** Logs at 40 (black) and 60 km (red) distance down-system. Also displayed is a filtered sedimentary log taken from Lascuarre in the Tremp Basin (Fig. 1, Michael et al. 2014b). **C)** Logs at 70 (black) and 90 km (red) distance down-system. Also displayed is a filtered sedimentary log from the Ainsa Basin (Fig. 1; Michael et al. 2014b). The three sedimentary logs have been filtered using a Gaussian filter with a window of 50 m, in order to highlight the main trends in the spatial distribution of fines, sand, and gravel grain sizes.

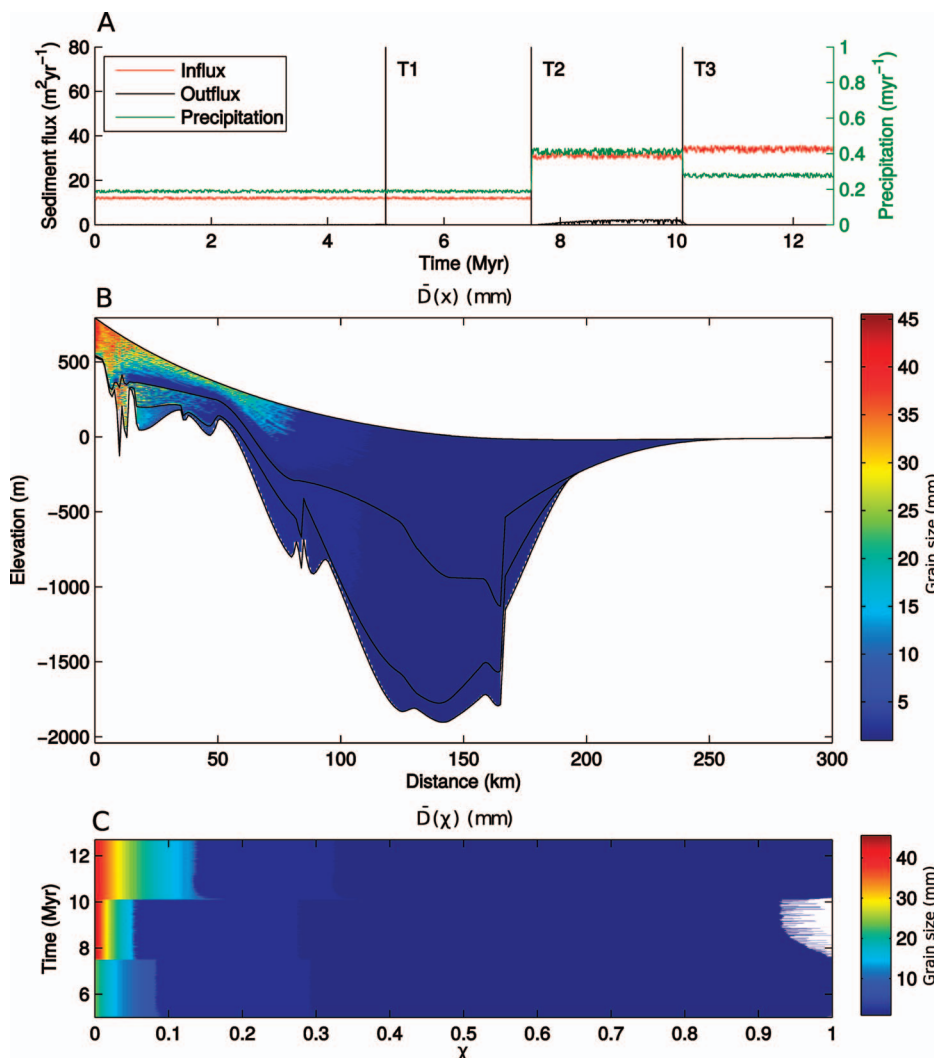


FIG. 11.—Stratigraphic architecture predicted by the forward model run that most closely matches the observed location of the gravel front adjusted for perfect sorting (Fig. 9) but with the addition of a small, 1% variation in the precipitation rate and sediment flux. A) Sediment flux in and out of the basin and precipitation rate against time. B) Distribution of mean grain size deposited in the idealized Escanilla paleo-sediment-routing system. C) Distribution of mean grain-size in mass-balance space. Note how the spatial variation in the gravel-front location in individual time intervals is masked. Furthermore there is a small amount of basin bypass in T2 marked by the white region at high values of  $\chi$ .

The model can predict the gross trend of gravel deposition increasing towards the end of T3 but cannot match the more detailed changes in deposition from fines to sands during time intervals T1 and T2 (Fig. 10). The progradation during T3 is a function of a steady sediment flux accompanied by a reduction in transport capacity. This causes a transient increase in slope at the catchment outlet, the left boundary. To accommodate this increased transport slope there is an increase in elevation and hence deposition at this boundary. The system then progrades again towards steady-state conditions that are representative of the distribution of accommodation (cf. Armitage et al. 2011). The stratigraphic architecture therefore reflects the relationship between flux of the sediment supply and transport capacity.

#### *Small Variations in System Forcing*

Given that the flux of the sediment supply and precipitation rate can act together to cause progradation and retrogradation, we have added noise of a magnitude 1% of the magnitude of the input signal to both precipitation rate and input sediment flux in order to visualize any high-frequency stratigraphic variations (Figs. 11, 12). The signal-to-noise ratio is small (Fig. 11A), but the resulting stratigraphic architecture shows a noticeable variation in grain-size (Figs. 11B, 12). This is because the change in the flux of the sediment supply and precipitation rate may either enhance progradation or reduce it, depending on whether peaks in these input signals coincide or

not. When transformed into mass-balance coordinates, the spatial variation is removed as the mass-balance space accounts for changes in the flux of the sediment supply and depositional thickness (Fig. 11C).

A qualitative comparison with the sedimentary logs suggests that the model with a small variation in the precipitation rate and the flux of the sediment input shows an improved correlation with the observations (Fig. 12B, C). The gross trend of prograding gravel deposits during T3 remains, but there is now also an increase in coarser deposits during T2, which corresponds with the increased abundance of sandstones observed during T2 at Lascuarre and Ainsa (Fig. 12B, C).

#### IMPLICATIONS FOR SEQUENCE STRATIGRAPHY

The physical sediment transport model used in this study, and the chronostratigraphic resolution of the Escanilla paleo-sediment-routing system, limits our results to stratigraphic architectures developed over several million years (cf. third-order sequences of Van Wagoner et al. 1990). Model runs generate synthetic patterns of grain-size distributions that resemble retrogradation and progradation of facies belts at this temporal scale. For example, a change from retrogradation to progradation of grain-size belts is found at the transition from T2 to T3, as revealed by synthetic logs (Figs. 10, 12) and cross-sectional basin profiles (Figs. 9, 11). These stratigraphic patterns were generated by the physical model through the interplay between the transport capacity of the

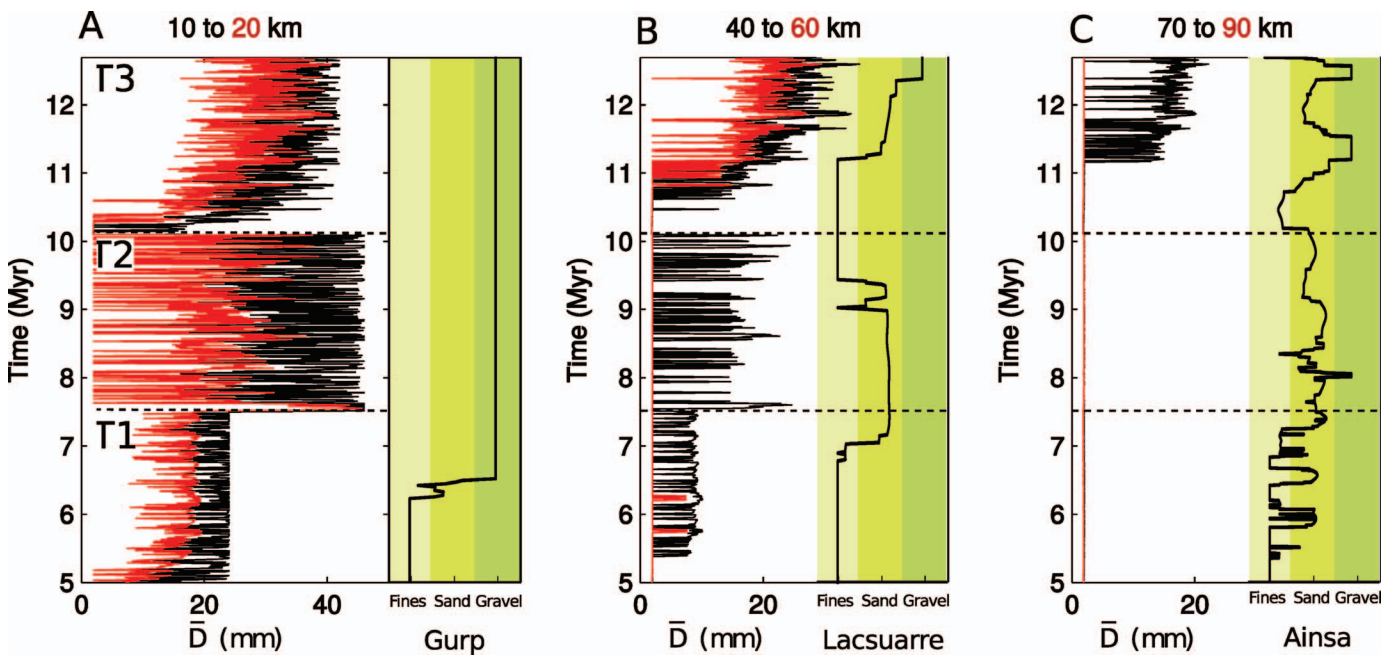


FIG. 12.—Synthetic sedimentary logs taken at six distances down-system where there is a small 1% variation in the input sediment flux and precipitation rate magnitude (see Fig. 11). **A**) Logs at 10 (black) and 20 km (red) distance down-system. Also displayed is a filtered sedimentary log taken from the Gurp escarpment in the Pobla Basin (Fig. 1; Michael et al. 2014b). **B**) Logs at 40 (black) and 60 km (red) distance down-system. Also displayed is a filtered sedimentary log taken from Lacsuarre in the Tremp Basin (Fig. 1; Michael et al. 2014b). **C**) Logs at 70 (black) and 90 km (red) distance down-system. Also displayed is a filtered sedimentary log from the Ainsa Basin (Fig. 1; Michael et al. 2014b). The three sedimentary logs have been filtered using a Gaussian filter with a window of 50 m, in order to highlight the main trends in the spatial distribution of fines, sand, and gravel grain sizes.

sediment-routing system, the supply of sediment from upland catchments, and the creation of accommodation space. In this context, movement of the gravel front proves to be a sensitive index of sediment-routing-system dynamics that allows the roles of sediment supply and accommodation generation as forcing mechanisms to be tested in the Escanilla sediment routing system (Figs. 5, 6). In order to reproduce the position of the gravel front in time intervals T1, T2, and T3, the sediment flux and transport capacity of the system must have changed at the transition between the time intervals (Fig. 9). Changes in accommodation and base level are insufficient to generate the observed stratigraphic patterns of gravel-front position.

The role of sediment supply in generating sequence stratigraphic architectures has long been recognized (e.g., Galloway 1989; Van Wagoner et al. 1990; Heller et al. 1993; Schlager 1993; Carvajal and Steel 2006; Carvajal et al. 2008). However, the use of a physical sediment transport model initialized and tested by observations from a well-documented case study enables the processes controlling sediment supply to be investigated quantitatively, and provides powerful support for the value of considering multiple controls on sequence architectures (e.g., “complexity paradigm” of Miall and Miall 2001). Unless the full sediment budget is known and placed within a sediment-routing-system context, interpretation and inversion of forcing mechanisms from stratigraphic observations is likely to suffer strongly from non-uniqueness. These results emphasize that the uncritical interpretation of a dominant accommodation control on sequence architecture (e.g., due to relative sea-level or base-level changes) may be misleading, particularly in the absence of a source-to-sink context and/or data that independently constrain sediment supply.

#### CONCLUSIONS

Stratigraphic architectures are controlled by the interplay at different spatial and temporal scales of accommodation generation and the magnitude and

grain-size mix of the sediment supply to a depositional basin. We have developed a simple 1-D sediment transport model that is initialized and constrained by data from the Eocene Escanilla sediment-routing system of the southern Pyrenees of northern Spain, where a sediment budget for the source-to-sink system has been evaluated previously. In the physical sediment transport model, transport capacity is a linear function of the local slope and the water flux, and the sediment flux of the input is estimated as that required to generate the observed stratigraphic thicknesses. Grain-size in the basin is calculated using a Sternberg-type exponential rule driven by selective deposition.

The Escanilla paleo-sediment-routing system is divided into three time intervals, T1 to T3, each of approximately 2.6 Myr duration, characterized by different magnitudes of the sediment supply. Field observations show that there was a temporal increase in the sediment flux from T1 to T3. A best-fit model was found by running 300 model simulations with different values of precipitation and transport coefficient, and testing model outcomes with the observed position of the gravel front. The increase in sediment input from time interval T1 to time interval T2 was accompanied by shortening of the distance from the catchment outlet to the gravel front, most likely caused by an increase in precipitation causing higher water fluxes, which is consistent with paleoclimate information from the mid-to-late Eocene. The gravel-front extended down-system during T3. To explain this new gravel front position while maintaining the sediment flux at the level to explain stratigraphic thicknesses, the transport capacity is required to decrease. This is best explained by a reduction in precipitation in time interval T3, which again matches with paleoclimate proxies in the late Eocene.

Shifting of the position of moving boundaries such as the gravel front is accompanied by patterns of retrogradation and progradation of grain-size trends. Such patterns, which are analogous to shoreline and shelf-break trajectories, are used as a standard tool in characterizing sequence stratigraphic patterns and assessing their forcing mechanisms. We find that patterns of retrogradation and progradation that match field observations can be generated by changes in sediment flux and transport capacity without recourse to any

change in accommodation (e.g., due to changes in base level). Such an interpretation of a sediment-supply control is impossible without the context of a sediment-routing system and associated sediment budget. The absence of these sediment-supply constraints magnifies the non-uniqueness of solutions for forcing mechanisms derived by the interpretation or inversion of stratigraphic architectures.

#### ACKNOWLEDGMENTS

This work was funded by a Royal Astronomical Society Research Fellowship awarded to JJA. Work on the Escanilla system began through funding for a generic sediment-routing-system program generously provided by Statoil to PAA and through a doctoral project by NAM funded in part by Saudi Aramco. We thank Jeremiah Moody (Chevron Energy Technology Company) and Ron Steel (University of Texas) for very thorough and helpful reviews.

#### REFERENCES

- ALLEN, P.A., ARMITAGE, J.J., WHITTAKER, A.C., MICHAEL, N.A., RODA-BOLUDA, D., AND D'ARCY, M., 2015, Fragmentation model of the grain-size mix of sediment supplied to basins: *Journal of Geology*, v. 123, p. 405–427.
- ARMITAGE, J.J., DULLER, R.A., WHITTAKER, A.C., AND ALLEN, P.A., 2011, Transformation of tectonic and climatic signals from source to sedimentary archive: *Nature Geoscience*, v. 4, p. 231–235.
- ARMITAGE, J.J., DUNKLEY JONES, T., DULLER, R.A., WHITTAKER, A.C., AND ALLEN, P.A., 2013, Temporal buffering of climate-driven sediment flux cycles by transient catchment response: *Earth and Planetary Science Letters*, v. 369–370, p. 200–210.
- ARMITAGE, J.J., DULLER, R.A., AND SCHMALHOLZ, S.M., 2014, The influence of long-wavelength tilting and climatic change on sediment accumulation: *Lithosphere*, v. 6, p. 303–318.
- BEAMUD, E., MUÑOZ, J.A., FITZGERALD, P.G., BALDWIN, S.L., GARCÉS, M., CABRERA, L., AND METCALF, J.R., 2010, Magnetostratigraphy and detrital apatite fission track thermochronology in syntectonic conglomerates: constraints on the exhumation of the south-central Pyrenees: *Basin Research*, v. 13, p. 309–331.
- BENTHAM, P.A., AND BURBANK, D.W., 1996, Chronology of Eocene foreland basin evolution along the western margin of the south-central Pyrenees, in Friend, P.F., and Dabrio, C.J., eds., *Tertiary Basins of Spain: the Stratigraphic Record of Crustal Kinematics*: Cambridge, U.K., Cambridge University Press, p. 144–152.
- BENTHAM, P.A., BURBANK, D.W., AND PUIGDEFABREGAS, C., 1992, Temporal and spatial controls on the alluvial architecture of an axial drainage system: late Eocene Escanilla Formation, southern Pyrenean foreland basin, Spain: *Basin Research*, v. 4, p. 335–352.
- BURGESS, P.M., AND PRINCE, G.D., 2015, Non-unique stratigraphic geometries: implications for sequence stratigraphic interpretations: *Basin Research*, v. 27, p. 351–365.
- BURT, T.J., AND ALLISON, R.J., 2010, Sediment cascades, in Burt, T.J., and Allison, R.J., eds., *Sediment Cascades in the Environment: an Integrated Approach*: Chichester, U.K., John Wiley and Sons, p. 1–15.
- CARVAJAL, C.R., AND STEEL, R.J., 2006, Thick turbidite successions from supply-dominated shelves during sea-level highstand: *Geology*, v. 34, p. 665–668.
- CARVAJAL, C., AND STEEL, R.J., 2012, Source-to-sink sediment volumes within a tectonistratigraphic model for a Laramide shelf-to-deep-water basin: methods and results, in Busby, C., and Azor, A., eds., *Tectonics of Sedimentary Basins: Recent Advances*: Oxford, U.K., Blackwell Publishing, p. 131–151.
- CARVAJAL, C., STEEL, R.J., AND PETTER, A.L., 2008, Sediment supply: the main driver of shelf-margin growth: *Earth-Science Reviews*, v. 96, p. 221–248.
- CATUNEANU, O., ABREU, V., BHATTACHARYA, J.P., BLUM, M.D., DALRYMPLE, R.W., ERIKSSON, P.G., FIELDING, C.R., FISHER, W.L., GALLOWAY, W.E., GIBLING, M.R., GILES, K.A., HOLBROOK, J.M., JORDAN, R., KENDALL, C.G., MACURDA, B., MARTINSEN, O.J., MIALL, A.D., NEAL, J.E., NUMMEDAL, D., POMAR, L., POSAMENTIER, H.W., PRATT, B.R., SARG, J.F., SHANLEY, K.W., STEEL, R.J., STRASSER, A., TUCKER, M.E., AND WINKER, C., 2009, Towards the standardization of sequence stratigraphy: *Earth-Science Reviews*, v. 92, p. 1–33.
- CAVAGNETTO, C., AND ANADÓN, P., 1996, Preliminary palynological data on floristic and climatic changes during the middle Eocene–early Oligocene of the eastern Ebro basin, northeast Spain: Review of Palaeobotany and Palynology, v. 92, p. 281–305.
- DENSMORE, A.L., ALLEN, P.A., AND SIMPSON, G., 2007, Development and response of a coupled catchment fan system under changing tectonic and climatic forcing: *Journal of Geophysical Research*, v. 112 (F01002), doi: 10.1029/2006JF000474.
- DULLER, R.A., WHITTAKER, A.C., FEDELE, J.J., WHITCHURCH, A.L., SPRINGETT, J., SMITHILLS, R., FORDYCE, S., AND ALLEN, P.A., 2010, From grain size to tectonics: *Journal of Geophysical Research*, v. 115 (F03022), doi: 10.1029/2009JF001495.
- DREYER, T., CORREGIDOR, J., ARBUES, P., AND PUIGDEFABREGAS, C., 1999, Architecture of the tectonically influenced Sobrarbe deltaic complex in the Ainsa Basin, northern Spain: *Sedimentary Geology*, v. 127, p. 127–169.
- FEDELE, J.J., AND PAOLA, C., 2007, Similarity solutions for alluvial sediment fining by selective deposition: *Journal of Geophysical Research*, v. 112 (F02038), doi: 10.1029/2005JF000409.
- FLEMINGS, P.B., AND JORDAN, T.E., 1989, A synthetic stratigraphic model of foreland basin development: *Journal of Geophysical Research*, v. 94, p. 3851–3866, doi: 10.1029/JB094iB04p03851.
- GALLOWAY, W.E., 1989, Genetic stratigraphic sequences in basin analysis I: architecture and genesis of flooding-surface bounded depositional units: *American Association of Petroleum Geologists, Bulletin*, v. 73, p. 125–142.
- GRADSTEIN, F.M., OGG, J.G., AND SMITH, A.G., eds., 2004, *A Geologic Time Scale 2004*: Cambridge, U.K., Cambridge University Press, 589 p.
- GUISSEPE, A.C., AND HELLER, P.L., 1998, Long-term river response to regional doming in the Price River Formation, central Utah: *Geology*, v. 26, p. 239–242.
- HARBAUGH, J.W., WATNEY, W.L., RANKEY, E.C., SLINGERLAND, R., GOLDSTEIN, R.H., AND FRANSEEN, E.K., 1999, Numerical Experiments in Stratigraphy: Recent Advances in Stratigraphic and Sedimentologic Computer Simulation: SEPM, Special Publication 62, 362 p.
- HAQ, B.U., HARDENBOL, J., AND VAIL, P.R., 1987, Chronology of fluctuating sea levels since the Triassic: *Science*, v. 235, p. 1156–1167.
- HELLAND-HANSEN, W., AND HAMPSON, G.J., 2009, Trajectory analysis: concepts and applications: *Basin Research*, v. 21, p. 454–483.
- HELLAND-HANSEN, W., AND MARTINSEN, O.J., 1996, Shoreline trajectories and sequences: description of variable depositional-dip scenarios: *Journal of Sedimentary Research*, v. 66, p. 670–688.
- HELLER, P.L., BURNS, B.A., AND MARZO, M., 1993, Stratigraphic solution sets for determining the roles of sediment supply, subsidence, and sea level on transgressions and regressions: *Geology*, v. 21, p. 747–750.
- HOLBROOK, J., SCOTT, R.W., AND OBOH-IKUNOBE, F.E., 2006, Base-level buffers and buttresses: a model for upstream versus downstream control on fluvial geometry and architecture within sequences: *Journal of Sedimentary Research*, v. 76, p. 162–174.
- MARR, J.G., SWENSON, J.G., PAOLA, C., AND VOLLER, V.R., 2000, A two-diffusion model of fluvial stratigraphy in closed depositional basins: *Basin Research*, v. 12, p. 381–398.
- MARTIN, J., PAOLA, C., ABREU, V., NEAL, J., AND SHEETS, B., 2009, Sequence stratigraphy of experimental strata under known conditions of differential subsidence and variable base level: *American Association of Petroleum Geologists, Bulletin*, v. 93, p. 503–533.
- MARTIN, Y., AND CHURCH, M., 1997, Diffusion in landscape development models: on the nature of basic transport relations: *Earth Surface Processes and Landforms*, v. 22, p. 273–279.
- MARTINSEN, O.J., RYSETH, A., HELLAND-HANSEN, W., FLESCHE, H., TORKILDSEN, G., AND IDIL, S., 1999, Stratigraphic base level and fluvial architecture: Ericson Sandstone (Campanian), Rock Springs Uplift, SW Wyoming, USA: *Sedimentology*, v. 46, p. 235–259.
- MARZO, M., AND STEEL, R.J., 2000, Unusual features of sediment supply-dominated, transgressive-regressive sequences: Paleogene clastic wedges, SE Pyrenean foreland basin, Spain: *Sedimentary Geology*, v. 138, p. 3–15.
- MIAILL, A.D., AND MIAILL, C.E., 2001, Sequence stratigraphy as a scientific enterprise: the evolution and persistence of conflicting paradigms: *Earth-Science Reviews*, v. 54, p. 321–348.
- MICHAEL, N.A., 2013, Functioning of an ancient sediment routing system, the Escanilla Formation, south-central Pyrenees [Ph.D. thesis]: Imperial College London, 318 p.
- MICHAEL, N.A., WHITTAKER, A.C., AND ALLEN, P.A., 2013, The functioning of sediment routing systems using a mass balance approach: example from the Eocene of the Southern Pyrenees: *Journal of Geology*, v. 121, p. 581–606.
- MICHAEL, N.A., CARTER, A., WHITTAKER, A.C., AND ALLEN, P.A., 2014a, Erosion rates in the source region of an ancient sediment routing system: comparison of depositional volumes with thermochronometric estimates: *Geological Society of London, Journal*, v. 171, p. 401–412.
- MICHAEL, N.A., WHITTAKER, A.C., CARTER, A., AND ALLEN, P.A., 2014b, Volumetric budget and grain-size fractionation of a geological sediment routing system: Eocene Escanilla Formation, south-central Pyrenees: *Geological Society of America, Bulletin*, v. 126, p. 585–599.
- MILLER, K.G., KOMINZ, M.A., BROWNING, J.V., WRIGHT, J.D., MOUNTAIN, G.S., KATZ, M.E., SUGARMAN, P.J., CRAMER, B.S., CHRISTIE-BLICK, N., AND PEKAR, S.F., 2005, The Phanerozoic record of global sea-level change: *Science*, v. 310, p. 1293–1298.
- MUÑOZ, J.A., 1992, Evolution of a continental collision belt: ECORS, Pyrenees crustal balanced section, in McClay, K.R., ed., *Thrust Tectonics*: London, Chapman and Hall, p. 235–246.
- MUÑOZ, J.A., BEAMUD, E., FERNÁNDEZ, O., ARBUÉS, P., DINARÉS-TURELL, J., AND POBLET, J., 2013, The Ainsa Fold and Thrust Oblique Zone: kinematics of a curved contractional system from paleomagnetic and structural data: *Tectonics*, v. 32, p. 1142–1175.
- MUTO, T., AND STEEL, R.J., 1997, Principles of regression and transgression: the nature of the interplay between accommodation and sediment supply: *Journal of Sedimentary Research*, v. 67, p. 994–1000.
- MUTO, T., AND STEEL, R.J., 2000, The accommodation concept in sequence stratigraphy: some dimensional problems and possible redefinition: *Sedimentary Geology*, v. 130, p. 1–10.
- NUMAN, W., 1998, Cyclicity and basin axis shift in a piggyback basin: towards modelling of the Eocene Tremp–Ager Basin, South Pyrenees, Spain, in Mascole, A., Puigdefàbregas, C., Luterbacher, H.P., and Fernández, M., eds., *Cenozoic Foreland Basins of Western Europe*: Geological Society of London, Special Publication 134, p. 135–162.
- PAOLA, C., AND MARTIN, J.M., 2012, Mass-balance effects in depositional systems: *Journal of Sedimentary Research*, v. 82, p. 435–450.
- PAOLA, C., AND SEAL, R., 1995, Grain-size patchiness as a cause of selective deposition and downstream fining: *Water Resources Research*, v. 31, p. 1395–1407.
- PAOLA, C., HELLER, P.L., AND ANGEVINE, C.L., 1992, The large-scale dynamics of grain-size variation in alluvial basins, 1: Theory: *Basin Research*, v. 4, p. 73–90.
- PAOLA, C., STRAUB, K., MOHRIG, D., AND REINHARDT, L., 2009, The “unreasonable effectiveness” of stratigraphic and geomorphic experiments: *Earth-Science Reviews*, v. 97, p. 1–43.
- PUIGDEFABREGAS, C., MUÑOZ, J.A., AND VERGÉS, J., 1992, Thrusting and foreland basin evolution in the southern Pyrenees, in McClay, K.R., ed., *Thrust Tectonics*: London, Chapman and Hall, p. 247–254.
- SCHLAGER, W., 1993, Accommodation and supply: a dual control on stratigraphic sequences: *Sedimentary Geology*, v. 86, p. 111–136.
- SHANLEY, K.W., AND McCABE, P.J., 1994, Perspectives on the sequence stratigraphy of continental strata: *American Association of Petroleum Geologists, Bulletin*, v. 78, p. 544–568.

- SIMPSON, G., AND SCHLUNEGGER, F., 2003, Topographic evolution and morphology of surfaces evolving in response to coupled fluvial and hillslope sediment transport: *Journal of Geophysical Research*, v. 108 (B62300), doi: 10.1029/2002JB002162.
- SINCLAIR, H.D., COAKLEY, B.J., ALLEN, P.A., AND WATTS, A.B., 1991, Simulation of foreland basin stratigraphy using a diffusion-model of mountain belt uplift and erosion: an example from the central Alps, Switzerland: *Tectonics*, v. 10, p. 599–620.
- SMITH, T.R., AND BRETHERTON, F.P., 1972, Stability and conservation of mass in drainage basin evolution: *Water Resources Research*, v. 8, p. 1506–1529.
- STEEL, R., AND OLSEN, T., 2002, Clinoforms, clinoform trajectories, and deepwater sands, in Armentrout, J.M., and Rosen, N.C., eds., *Sequence Stratigraphic Models for Exploration and Production: Evolving Methodology, Emerging Models and Applications Histories*: SEPM, Gulf Coast Section, 22nd Annual Research Conference, p. 367–380.
- STERNBERG, H., 1875, Untersuchungen über Längen und Querprofil geschiebeführende Flüsse: *Zeitschrift für das Bauwesen*, v. 25, p. 483–506.
- STRONG, N., SHEETS, B., HICKSON, T., AND PAOLA, C., 2005, A mass-balance framework for quantifying downstream changes in fluvial architecture, in Blum, M.D., Marriott, S.B., and Leclair, S.F., eds., *Fluvial Sedimentology VII*: Oxford, UK, Blackwell Publishing, v. 35, p. 243–253.
- SWENSON, J.B., 2005, Relative importance of fluvial input and wave energy in controlling the timescale for distributary-channel avulsion: *Geophysical Research Letters*, v. 32 (L23404), doi: 10.1029/2005GL024758.
- VAIL, P.R., MITCHUM, R.M., JR., TODD, R.G., WIDMIER, J.M., THOMPSON, S., III, SANTEE, J.B., BUBB, J.N., AND HATLELID, W.G., 1977, Seismic stratigraphy and global changes of sea level, *Geological Society of America Special Paper*, v. 227, p. 1–100.
- in Payton, C.E., ed., *Seismic Stratigraphy Applications to Hydrocarbon Exploration*: American Association of Petroleum Geologists, Memoir, v. 26, p. 49–212.
- VAN WAGONER, J.C., MITCHUM, R.M., CAMPION, K.M., AND RAHMANIAN, V.D., 1990, Siliciclastic Sequence Stratigraphy in Well Logs, Cores, and Outcrops: Association of Petroleum Geologists, Methods in Exploration 7, 55 p.
- VINCENT, S.J., 2001, The Sis palaeovalley: a record of proximal fluvial sedimentation and drainage basin development in response to Pyrenean mountain building: *Sedimentology*, v. 48, p. 1235–1276.
- WHITCHURCH, A.L., CARTER, A., SINCLAIR, H.D., DULLER, R.A., WHITTAKER, A.C., AND ALLEN, P.A., 2011, Sediment routing system evolution within a diachronously uplifting orogen: insights from detrital zircon thermochronological analyses from the south-central Pyrenees: *American Journal of Science*, v. 311, p. 442–482.
- WHITTAKER, A.C., DULLER, R.A., SPRINGETT, J., SMITHILLS, R.A., WHITCHURCH, A.L., AND ALLEN, P.A., 2011, Decoding downstream trends in stratigraphic grain-size as a function of tectonic subsidence and sediment supply: *Geological Society of America, Bulletin*, v. 123, p. 1363–1382.
- WILLIS, B.J., 1993, Ancient river systems in the Himalayan foredeep, Chinji Village area, northern Pakistan: *Sedimentary Geology*, v. 88, p. 1–76.
- WRIGHT, V.P., AND MARRIOTT, S.B., 1993, The sequence stratigraphy of fluvial depositional systems: the role of floodplain sediment storage: *Sedimentary Geology*, v. 86, p. 203–210.

Received 6 February 2015; accepted 7 October 2015.